

RL-TR-91-244  
Final Technical Report  
September 1991

AD-A243 121



2

# INVESTIGATION OF MICROWAVE MONOLITHIC INTEGRATED CIRCUIT (MMIC) NON-RECIPROCAL MILLIMETER- WAVE COMPONENTS

Westinghouse Science & Technology Center

S.H. Talisa, S.V. Krishnaswamy, J.D. Adam, K.C. Yoo,  
N.J. Doyle

DTIC  
ELECTE  
DEC 10 1991  
S D D

*APPROVED FOR PUBLIC RELEASE; DISTRIBUTION UNLIMITED.*

91-17365



91 1209 031

Rome Laboratory  
Air Force Systems Command  
Griffiss Air Force Base, NY 13441-5700

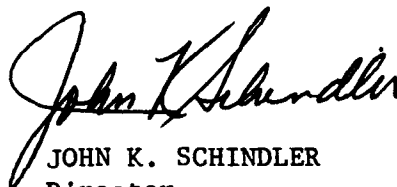
This report has been reviewed by the Rome Laboratory Public Affairs Office (PA) and is releasable to the National Technical Information Service (NTIS). At NTIS it will be releasable to the general public, including foreign nations.

RL-TR-91-244 has been reviewed and is approved for publication.

APPROVED: 

PETER J. RAINVILLE  
Project Engineer

FOR THE COMMANDER:



JOHN K. SCHINDLER  
Director  
Electromagnetics & Reliability Directorate

If your address has changed or if you wish to be removed from the Rome Laboratory mailing list, or if the addressee is no longer employed by your organization, please notify RL( ERAC ) Hanscom AFB MA 01731-5000. This will assist us in maintaining a current mailing list.

Do not return copies of this report unless contractual obligations or notices on a specific document require that it be returned.

# REPORT DOCUMENTATION PAGE

Form Approved  
OMB No. 0704-0188

Public reporting burden for this collection of information is estimated to average 1 hour per response, including the time for reviewing instructions, searching existing data sources, gathering and maintaining the data needed, and completing and reviewing the collection of information. Send comments regarding this burden estimate or any other aspect of this collection of information, including suggestions for reducing this burden, to Washington Headquarters Services, Directorate for Information Operations and Reports, 1215 Jefferson Davis Highway, Suite 1204, Arlington, VA 22202-4302, and to the Office of Management and Budget, Paperwork Reduction Project (0704-0188), Washington, DC 20503.

1. AGENCY USE ONLY (Leave Blank)		2. REPORT DATE September 1991		3. REPORT TYPE AND DATES COVERED Final Mar 87 - Jan 90	
4. TITLE AND SUBTITLE INVESTIGATION OF MICROWAVE MONOLITHIC INTEGRATED CIRCUIT (MMIC) NON-RECIPROCAL MILLIMETER-WAVE COMPONENTS				5. FUNDING NUMBERS C - F19628-87-C-0101 PE - 61102F PR - 2305 TA - J5 WU - 45	
6. AUTHOR(S) S. H. Talisa, S. V. Krishnaswamy, J. D. Adam, K. C. Yoo, N. J. Doyle					
7. PERFORMING ORGANIZATION NAME(S) AND ADDRESS(ES) Westinghouse Science & Technology Center 1310 Beulah Road Pittsburgh PA 15235				8. PERFORMING ORGANIZATION REPORT NUMBER N/A	
9. SPONSORING/MONITORING AGENCY NAME(S) AND ADDRESS(ES) Rome Laboratory (ERAC) Hanscom AFB MA 01731-5000				10. SPONSORING/MONITORING AGENCY REPORT NUMBER RL-TR-91-244	
11. SUPPLEMENTARY NOTES Rome Laboratory Project Engineer: Peter J. Rainville/ERAC/(617) 377-4663					
12a. DISTRIBUTION/AVAILABILITY STATEMENT Approved for public release; distribution unlimited.				12b. DISTRIBUTION CODE	
13. ABSTRACT (Maximum 200 words) Two ferrite film deposition techniques were investigated in this program for possible use in the monolithic integration of GaAs electronic and magnetic millimeter-wave devices; (1) spin-spray plating (SSP) of nickel zinc ferrite films and (2) sputtering of barium hexaferrites with C-axis oriented normally to the film plane. The SSP technique potential for this application was demonstrated. Film structural characteristics were studied, as well as their adhesions to other substrates and the conditions for growth of thicker films. Multilayers totalling 25 $\mu$ m in thickness were grown on semiconducting substrates. The SSP process occurs at about 100°C and was experimentally demonstrated not to damage GaAs MMIC devices. The magnetic characteristics of these films were comparable to ceramic materials. A scheme for the monolithic integration of magnetic and GaAs electronic devices was proposed and its feasibility experimentally demonstrated. The films showed higher dielectric loss than was desirable, possibly owing to high water content. A better drying technique is required. Barium ferrite films with C-axis texture were reproducibly grown on sapphire. Magnetic measurements yielded acceptable saturation magnetization and anisotropy field. Ferromagnetic resonance was not observed, possibly due to broad linewidths.					
14. SUBJECT TERMS Microwaves, Monolithic, Integrated Circuits, MM-Wave, Components, Ferrites, Films, Yig, Nickel, Zinc, Hexagonal, Measurements, Frequency, Magnetic, Barium Ferrite				15. NUMBER OF PAGES 96	
				16. PRICE CODE	
17. SECURITY CLASSIFICATION OF REPORT UNCLASSIFIED		18. SECURITY CLASSIFICATION OF THIS PAGE UNCLASSIFIED		19. SECURITY CLASSIFICATION OF ABSTRACT UNCLASSIFIED	
				20. LIMITATION OF ABSTRACT SAR	

# SUMMARY

## OBJECTIVE

The objective of this program was to investigate techniques to integrate millimeter-wave ferrite devices with GaAs MMICs.

## APPROACH

Our approach was to deposit ferrite thin films on GaAs substrates in a manner compatible with the fabrication of electronic components, and to develop techniques for the integration of both types of devices in a monolithic fashion.

Work was concentrated on an investigation of two techniques to deposit polycrystalline ferrite thin films onto metallized GaAs wafers:

- (a) The spin-spray plating of spinel ferrite films.
- (b) The sputtering of Ba-hexaferrite thin films with c-axis textured orientation perpendicular to the plane of the film.

The spin-spray plating method uses very low temperatures ( $\sim 100^\circ\text{C}$ ) and is therefore compatible with GaAs devices. Spinel ferrites have a saturation magnetization high enough to be useful at low millimeter wavelengths (20 to 35 GHz) without requiring impractically high applied magnetic fields. The goal for the second approach was to obtain, through the c-axis orientation, a substantial perpendicular anisotropy field for operation at millimeter wavelengths (40 to 60 GHz) with relatively low applied bias fields. Sputtering of oriented hexagonal ferrites required high temperatures, which is, in principle, incompatible with GaAs devices; the ferrite film must therefore be deposited on an encapsulated and then metallized wafer before electronic device fabrication.

## RESULTS

The results obtained on the spin-spray plating are highly encouraging. A broad range of aspects of their use for the integration of magnetic and electronic devices was investigated. The following are the most significant results:

- The growth of Ni-Zn ferrite films was established. Film structural characteristics were studied, as well as their adhesion to various substrates and the conditions for growth of thick films.
- Deposition of ferrite films takes place at 100°C and therefore already fabricated GaAs devices would not be damaged. This was experimentally demonstrated.
- The SSP apparatus is very inexpensive and quite adaptable to production of a large number of wafers or to deposition over large surfaces, planar or otherwise.
- The process for growing thick films suitable for practical devices and their feasibility were demonstrated (25- $\mu$ m-thick film grown).
- The magnetic characteristics of SSP Ni-Zn ferrite films are excellent for practical devices and quite comparable to published results on ceramic samples (i.e.  $4\pi M_s \approx 5$  KG,  $\Delta H < 100$  Oe,  $\gamma \approx 3$  GHz/KOe).
- A scheme for the monolithic integration of magnetic and GaAs electronic devices was put forth. Its feasibility was experimentally demonstrated.

The main problem areas encountered are the following:

- The Ni-Zn ferrite films were found to have relatively low resistivity and high dielectric loss at microwave frequencies due to high water content. A process to remove the water is under development under internal funding. Preliminary measurements on treated films show a significant improvement in the microwave loss factor, from  $\tan \delta > 10$  to  $\tan \delta < 1$ .

- The film composition cannot be controlled as readily as with ceramic samples due to chemical equilibrium conditions particular to the SSP process. These conditions are not completely understood as yet. The films grown in this program had only a partial substitution of Ni and Zn for divalent iron. This may result in unwanted residual microwave loss due to conduction.

Our results on Ba-ferrite films on sapphire substrates show that we have established a reproducible growth technique yielding the highest degree of c-axis orientation in the direction perpendicular to the plane of the film ever reported. Further work is needed to produce thicker films which could be tested for their millimeter wave properties. Films grown on this program had excellent structural properties and vibrating-sample and torque magnetometer measurements gave acceptable saturation (3.4 KG) and anisotropy field (10 KOe) parameters. However, it was not possible to observe ferromagnetic resonance in them, an important condition for millimeter-wave work. We concluded that linewidths must be in excess of 300 Oe.

Accession For	
NTIS CR&D	<input checked="" type="checkbox"/>
DTIC TAB	<input type="checkbox"/>
Unannounced	<input type="checkbox"/>
Justification	
By	
Distribution/	
Availability Codes	
Dist	Availability or Special
A-1	



# CONTENTS

<u>Section</u>	<u>Page</u>
1. INTRODUCTION.....	1
2. SPIN-SPRAY PLATING.....	7
2.1 INTRODUCTION.....	7
2.2 FILM GROWTH PROCESS.....	8
2.2.1 SSP Apparatus.....	9
2.2.2 Film Growth.....	9
2.3 FILM CHARACTERIZATION.....	16
2.3.1 Microstructure and Composition.....	16
2.3.2 Magnetic Characterization.....	21
2.4 FILMS FOR DEVICE STRUCTURES.....	24
2.4.1 Thick Film Growth.....	26
2.4.2 Film-Substrate Adhesion Studies.....	28
2.4.3 Monolithic Integration of GaAs MMICs with Ferrite Devices.....	33
2.4.4 GaAs MMIC Compatibility Experiment.....	38
2.5 ELECTRICAL CHARACTERISTICS.....	43
2.5.1 Electrical Resistivity Measurements.....	45
2.5.2 Microwave Loss Measurements.....	52
2.6 CONCLUSION.....	58
3. SPUTTERING OF BARIUM FERRITE THIN FILMS.....	59
3.1 INTRODUCTION.....	59
3.2 FILM GROWTH.....	60
3.3 RESULTS.....	62
3.3.1 Magnetic Measurements.....	68
3.4 SUMMARY AND CONCLUSION.....	72
4. CONCLUSIONS.....	74
REFERENCES.....	77
ACKNOWLEDGMENTS.....	78

# FIGURES

<u>Figure</u>		<u>Page</u>
1	Prototype solid state radar module containing GaAs monolithic power amplifiers, LNAs, and phase shifters, as well as hybrid circulators.....	2
2	Magnetic biasing field ( $H_0$ ) required and circulator diameter for YIG as a function of center frequency.....	5
3	Magnetic biasing field ( $H_0$ ) required and circulator diameter for Ni-Zn ferrite as a function of center frequency.....	5
4	Center frequency of a barium ferrite circulator as a function of anisotropy field (top) and circulator diameter for the same range of center frequencies (bottom).....	6
5	Spin-spray plating (SSP) apparatus.....	10
6	Schematic diagram of the SSP apparatus.....	11
7	Effect of pH and reaction temperature on the formation of various kinds of precipitates (after reference 2).....	12
8	X-ray diffraction pattern of FeO(OH) obtained from the precipitated particles in the mixed solution resulting from the reaction and oxidizing solutions at 60°C and 85°C.....	14
9	X-ray diffraction pattern of Ni-Zn ferrite obtained from the precipitated particles in the mixed solution resulting from the reaction and oxidizing solutions at 95°C and 100°C.....	15
10	X-ray diffraction patterns for three different films showing the (110), (211), and (111) textured structures. These films were grown with substrate temperatures at 97, 94, and 102°C, respectively.....	17
11	A Ni-Zn ferrite film (2 in. x 3 in.) grown on a glass substrate.....	19



12	The (333) X-ray reflection spectra for three Ni-Zn ferrite films with compositions listed in Table 2.....	19
13	Perpendicular FMR spectra for samples from a) the wafer edge and b) the wafer center of film MW62 on gold-on-silicon.....	23
14	a) Perpendicular and b) parallel FMR data for sample MW63 (4 $\mu\text{m}$ ) on gold-on-GaAs. From these curves, $\gamma = 3.0 \text{ GHz/KOe}$ , $4\pi M_s = 5620 \text{ G}$ .....	25
15	SEM observation of the cross section of Ni-Zn ferrite films grown on GaAs, Si, and GGG.....	27
16	SEM photograph of the cross section of a multilayer Ni-Zn ferrite film on a gold-plated GaAs wafer. The film was grown in four separate depositions for a total of 8 hours. Its thickness is about 14 $\mu\text{m}$ .....	29
17	SEM photograph of the cross section of a multilayer Ni-Zn ferrite film on a gold-plated Si wafer. The film was grown in eight separate depositions for a total of 16 hours. Its thickness is about 25 $\mu\text{m}$ .....	29
18	X-Ray diffraction pattern for multilayer 25- $\mu\text{m}$ -thick Ni-Zn ferrite film on Au/Si, showing (111) textured structure.....	30
19	Perpendicular FMR spectrum for 25- $\mu\text{m}$ -thick multilayer Ni-Zn ferrite film on Au/Si. Multiple resonance peaks evidence small compositional nonuniformities among different layers.....	31
20	Ferrite films deposited at 97°C and grown on Si, on Au/Si, and on SiO <sub>2</sub> /Si.....	32
21	Ferrite films from a shorter deposition run (2.5 hrs) under the same conditions as Figure 20, but only on bare Si and on SiO <sub>2</sub> /Si.....	34
22	Monolithic integration of microwave magnetic and GaAs devices using spin-spray-plated ferrite films.....	35
23	SEM photograph showing etched cavity and pits on a test GaAs wafer used for an experiment of film deposition on nonplanar geometries.....	36
24	Ni-Zn ferrite film on (a) sloping wall of etched cavity on a GaAs wafer and (b) on steep walls of an etchpit.....	37

25	Photograph of GaAs Wafer Scale piece with three T/R modules showing two ferrite disks from deposited and patterned SSP ferrite multilayer films. The disks' diameter is that of a junction circulator of conventional design at 20 GHz. The wafer piece was mounted on a 3-inch diameter sapphire wafer for support.....	39
26	Photograph of fabricated wafer showing 16 T/R cells.....	40
27	Single cell from a 16 T/R cell wafer.....	41
28	Wafer map of maximum available gain (MAG) for the test P-FETs in each of the three T/R modules shown in Figure 25: (a) before and (b) after ferrite processing. Measurement parameters are indicated in the wafer maps.....	42
29	1,000X magnification of the gate areas of one of the test P-FETs showing residual photoresist between the gates and source and drain, thus degrading the transistor performance.....	43
30	Photograph of two-point probe dc resistivity measurement equipment.....	46
31	Photograph of sample with 15 pairs of gold contacts for dc resistivity measurements.....	47
32	Comparison of V-I characteristics for Ni-Zn ferrite film MW116 with those for a commercial sample and the glass substrate MW116 was grown on.....	48
33	Bar-graph of maximum resistivities ( $\Omega$ -cm) for SSP films measured.....	50
34	Schematic diagram of the experimental arrangement for dielectric loss measurements at 9.3 GHz. Measurements were made by comparing the film on its substrate with the substrate alone, after etching the film away.....	53
35	Example raw data from a $\tan \delta$ measurement of a 2- $\mu$ m-thick ferrite film. The film has a dc resistivity of 4000 $\Omega$ -cm.....	54
36	Dielectric loss tangent at 9.3 GHz as a function of dc resistivity for SSP Ni-Zn ferrite films.....	56
37	Loss tangent at 10 GHz versus dc resistivity for silicon material. Generated in an unrelated program, <sup>9</sup> this curve is included here for comparison with our results only.....	57
38	RF sputtering system used in this work.....	61

39	(a) Representative X-ray $\theta/2\theta$ scan from sputtered sample BAF-7, and (b) X-ray $\theta/2\theta$ scan of film BAF-39 showing c-axis texture. The large peak at $69^\circ$ is due to silicon substrate.....	64
40	X-ray oscillation photographs of RF-diode-sputtered barium ferrite films taken with CuK $\alpha$ radiation: (a) Film on SiO $_2$ /Si grown by Prof. Morisako; sample BM-156. (b) Film on platinum grown at Westinghouse; sample BAF-35-2. (c) Film on SiO $_2$ /Si grown at Westinghouse; sample BAF-39. It is clear from this photograph that using less-penetrating CrK $\alpha$ radiation enhances the (00 $l$ ) reflections.....	65
41	X-ray $\theta/2\theta$ scan for magnetron-sputtered barium ferrite film on sapphire. Post-deposition annealing was carried out in oxygen at 800°C. Insert shows the rocking curve for this film.....	66
42	Variation of half-width X-ray rocking curve [(008) peak] for magnetron-sputtered films deposited at different substrate temperatures. CuK $\alpha$ radiation was used.....	67
43	Vibrating sample magnetometer measurements: raw data for sample BAF-80 grown on sapphire by magnetron sputtering and post-deposition annealing. Film is 2,800 Å thick and sample measured was 7 mm by 7 mm. (a) Applied field perpendicular and (b) parallel to film plane.....	70
44	Torque magnetometer measurements: raw data for sample BAF-80 grown on sapphire by magnetron sputtering and post-deposition annealing. Film is 2,800 Å thick and sample measured was 7 mm by 7 mm. (a) Nickel wire reference and (b) BAF-80 sample.....	71

## TABLES

<u>Table</u>	<u>Page</u>
1     Plating Conditions Under Which Different Textured Structures Were Obtained.....	18
2     Aqueous Solutions Used for Studying the Composition Dependence of the Lattice Parameter.....	20
3     Film Composition and Lattice Parameters of Ferrite Films Grown from Different Solution Composition.....	20
4     Summary of FMR Characterization.....	22
5     Solution Compositions.....	51
6     Chemical Composition and Electrical Resistivity.....	51
7     Range of Deposition Parameters.....	62
8     Results of Analysis from Vibrating Sample and Torque Magnetometer Measurements on Different Samples of Sputtered Ba-Ferrite.....	69

# 1. INTRODUCTION

The objective of this program was to find ways to monolithically integrate millimeter-wave electronic GaAs and magnetic devices such as circulators and phase shifters. Our approach was to develop film deposition techniques that would allow growth of ferrite films onto GaAs wafers at sufficiently low temperatures to be compatible with fabricated electronic devices, or, alternatively, a method that would yield a good-quality ferrite film that could be deposited prior to electronic device fabrication if relatively high temperatures were required. Once a suitable deposition technique was established, the plan was to demonstrate its capabilities by building a microstrip junction circulator of conventional design.

Figure 1 is a photograph of a phased-array antenna element showing two circulators built using expensive hybrid technology. Cost is a major factor when considering systems like phased arrays, where thousands of identical modules are required. Notice also their large size compared to electronic devices. New designs based on monolithic circuit fabrication techniques can be developed once integration becomes possible. A prime candidate for this may be lumped-element circulators.

Growth of epitaxial (single crystal) thin films was not deemed necessary here since most microwave magnetic devices can be built using good-quality polycrystalline material. Since devices suitable for work at millimeter wavelengths were a stated goal for this program, the choice of hexagonal ferrites seemed logical. Their high crystalline anisotropy fields allow their use at high frequencies without the need for an impractically large applied magnetic field. In devices like planar circulators, the anisotropy axis (c-axis) must be perpendicular to the plane of the ferrite. We found the work of Professor Akimitsu Morisako, from Shinshu University in Japan, on deposition by sputtering c-axis-oriented barium ferrite films ideally suited to the goals of this program, given our extensive experience sputtering oxide materials. This approach was therefore adopted.

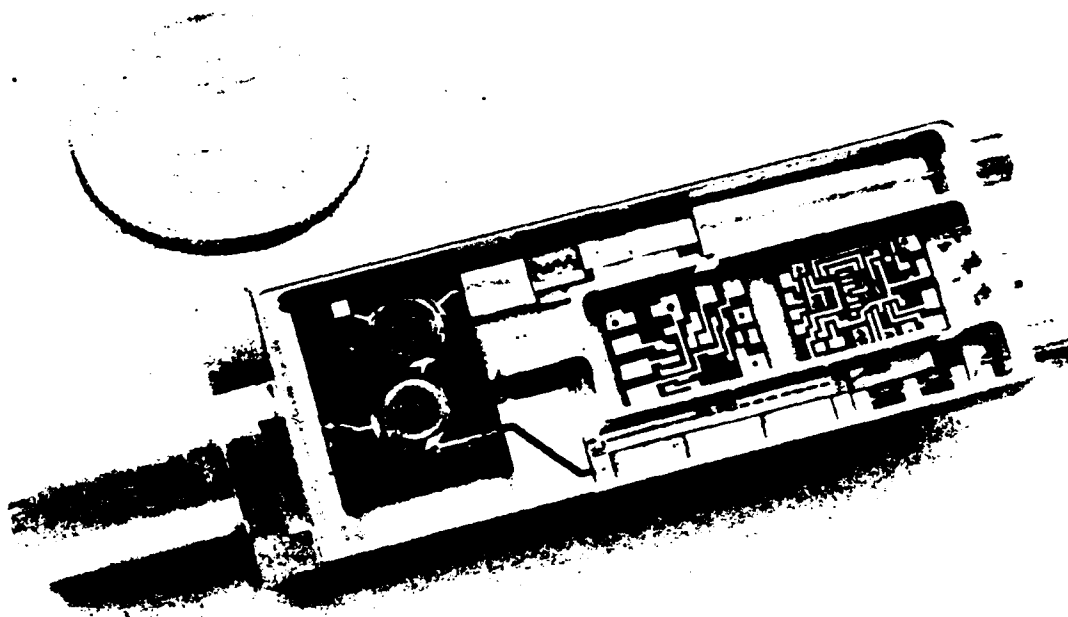


Figure 1. Prototype solid state radar module containing GaAs monolithic power amplifiers, LNAs, and phase shifters, as well as hybrid circulators.

A second approach was also adopted for deposition of spinel ferrites which, although not suited for work at high-millimeter-wave frequencies because of their small anisotropy field, they have a large saturation magnetization and are therefore usable in the 20 to 35 GHz range. A technique, first demonstrated by Professor Masanori Abe and co-workers from the Tokyo Institute of Technology in Japan, consisted of deposition of Ni-Zn ferrite layers by spin-spray plating at temperatures as low as 100°C on a large variety of substrates. Since crystalline texture orientation considerations for films of this material are of secondary importance because of their cubic structure, this technique was also chosen for our program. Films so deposited promised ready compatibility with already fabricated GaAs devices.

Both approaches were carried through to the end of the program. The latter, spin-spray plating (SSP) of Ni-Zn ferrite films, appeared more successful than the sputtering of barium ferrite films. Our results on both approaches, however, advanced the understanding and the possibility of monolithic integration of ferrite devices with GaAs electronic devices.

Our original intention was to first develop film deposition techniques and, toward the end of the program, demonstrate their use and quality by building a junction circulator. This was not possible in the end since both types of films presented problems which needed solving before a device demonstration was attempted. Thus, the SSP Ni-Zn ferrite films, which had excellent magnetic and structural characteristics and could be grown as very thick films, turned out to have very high dielectric losses. Our attention was best turned toward finding a solution to this problem. Although this was not possible by the end of the program, work performed under internal support immediately afterward yielded encouraging results and significant improvements in the loss characteristics of these films.

Of special significance in the SSP work is the fact that the equipment needed is very inexpensive compared to systems requiring high vacuum. It also is very adaptable to production of large numbers of wafers or coating of large areas, planar or otherwise.

Progress with the barium ferrite films was not as fast as originally planned. This is a very challenging area and we had difficulties

producing films with the required characteristics. Several research groups around the world have, over the years, tried unsuccessfully to grow hexagonal ferrite films usable in planar millimeter-wave devices. In this program, films with a very high degree of orientation were produced on sapphire substrates. Although their magnetic characteristics were satisfactory, it was not possible to observe ferromagnetic resonance in them, possibly due to very broad linewidths, even though the measurement equipment used was extremely sensitive.

Work throughout the program was directed toward demonstration of the planar circulator, especially in the case of SSP films. Thus, typical circulator dimensions were calculated from literature values of parameters for the different films. These calculations are presented in Figures 2 to 4 and include the case of YIG for comparison purposes. As for the films thicknesses required, this would be determined by the dimensions of the final design used and the configuration chosen to integrate the circulator with the electronic circuits. Typically, thicknesses on the order of 100  $\mu\text{m}$  or more were felt necessary for low conduction loss in the metallization. As will be seen, this appeared possible in the case of SSP films. The work on sputtering did not go so far as to show the feasibility of thick films, which could have been achieved by sputtering itself or by liquid-phase epitaxy on a presputtered thin film.

We first report on the SSP work and then on the sputtering of barium hexaferrite. At the end our recommendations for future work are given with a view to demonstrating practical devices.



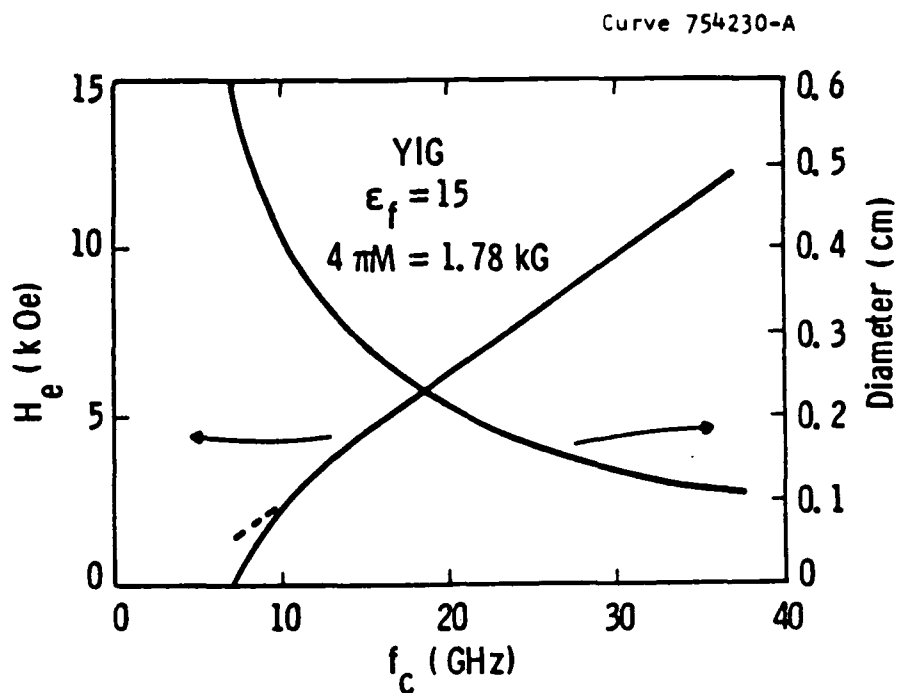


Figure 2. Magnetic biasing field ( $H_e$ ) required and circulator diameter for YIG as a function of center frequency.

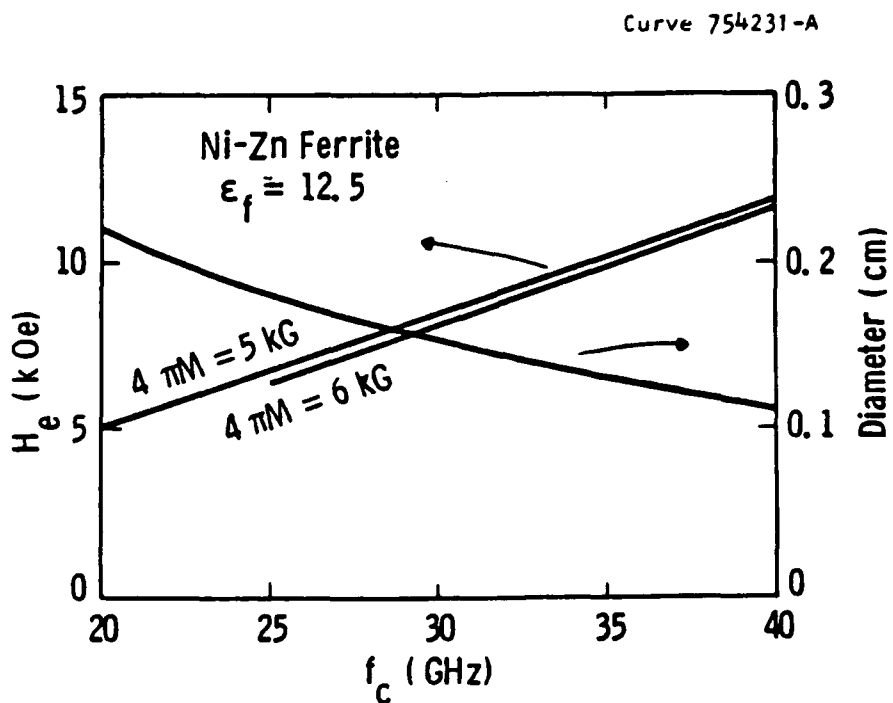


Figure 3. Magnetic biasing field ( $H_e$ ) required and circulator diameter for Ni-Zn ferrite as a function of center frequency.

Curve 754229-A

### BARIUM-FERRITE

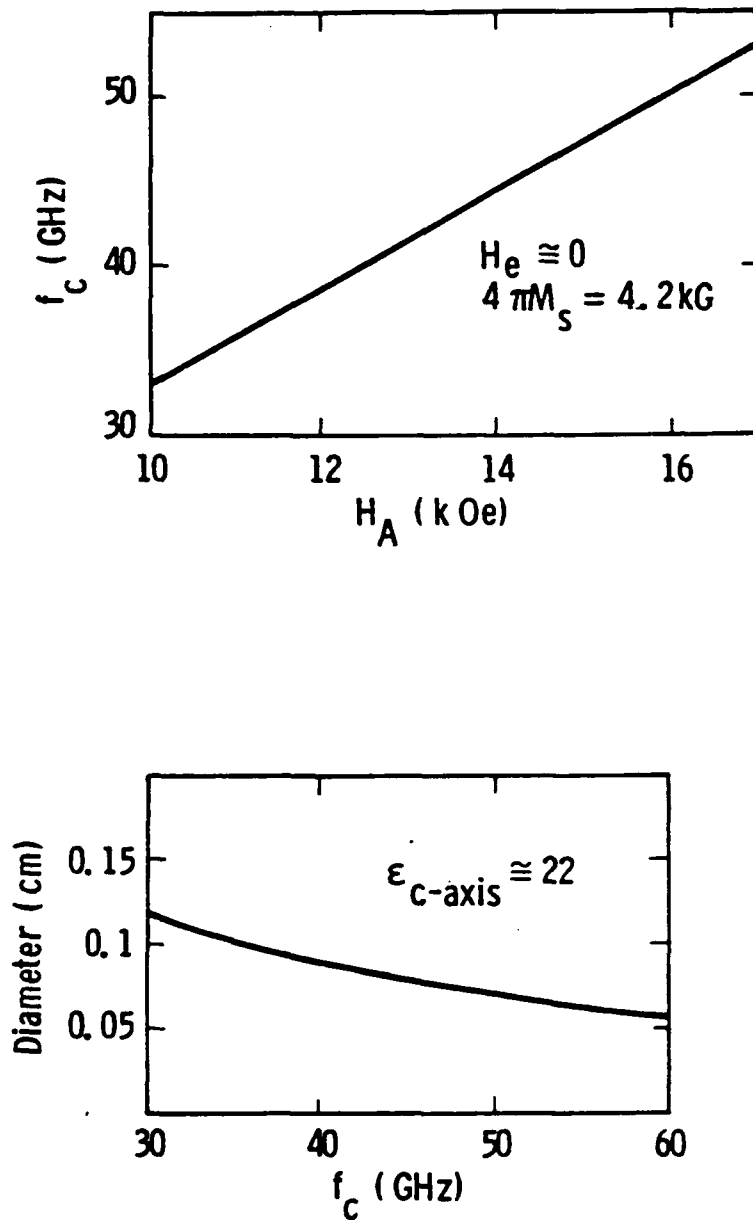


Figure 4. Center frequency of a barium ferrite circulator as a function of anisotropy field (top) and circulator diameter for the same range of center frequencies (bottom).

## 2. SPIN-SPRAY PLATING

### 2.1 INTRODUCTION

The Spin-Spray Plating (SSP) of ferrite films was studied in this program because of its great potential as a deposition technique compatible with GaAs integrated circuit fabrication. Ferrite films can be deposited by spraying aqueous solutions at temperatures as low as 100°C. This method was originally demonstrated by Professor M. Abe and his colleagues<sup>1</sup> from the Tokyo Institute of Technology in Japan. Dr. Abe helped us in the initial steps of setting up the plating apparatus in which the films for this program were grown.

We have used this method to prepare Ni-Zn spinel ferrite films on GaAs, Si, GGG, alumina, and glass substrates, in some cases with intermediate gold layers, to study the film properties under different growth conditions. The conditions required for the fabrication of non-reciprocal devices on the same wafer as GaAs MMICs were also studied. Since SSP is a low-temperature process (100°C), it facilitates deposition of ferrite materials onto GaAs substrates at any convenient stage in the device process sequence without any thermal deterioration of underlying GaAs device structures.

Ni-Zn ferrite has a high saturation magnetization (about 5000 G), making it suitable for devices in the range between 20 and 35 GHz. Although the films deposited are polycrystalline with a preferred orientation, the spinel ferrite has no appreciable magneto-crystalline anisotropy compared to the shape anisotropy ( $4\pi M_s$ ) because of its cubic structure. In contrast, hexagonal ferrites do have a very high anisotropy field (17 KOe for type-M hexagonal ferrites like barium ferrite) and are therefore usable at frequencies well in the millimeter-wave range.

Ni and Zn substitutions for divalent  $\text{Fe}^{2+}$  in  $\text{Fe}_3\text{O}_4$  (magnetite), giving Ni-Zn ferrite, form a microwave magnetic material ideally suited to the spin-spray technique. The reason is that  $\text{Fe}_3\text{O}_4$  and its derivatives

can be obtained from chemical reactions at temperatures as low as 40°C, thus satisfying the main objective of this effort, i.e., to grow ferrites at temperatures compatible with GaAs device fabrication.

In this report, a chronological approach will be taken to the description of the work performed. First, the growth process was developed, followed by the structural and magnetic characterization of the films obtained. Once the growth technique was established and the magnetic properties were seen to be quite good, our efforts turned toward obtaining films which could be used in device configurations; that is, adhesion to various substrates and the growth of very thick films were studied. An experiment to demonstrate the compatibility of the growth process with GaAs MMICs was run successfully. In addition, a possible processing sequence for the monolithic integration of magnetic and electronic devices in GaAs was proposed. Since this requires ferrite film growth on vertical walls defined on GaAs wafers, the feasibility of doing this was also successfully demonstrated. The electrical characteristics of the SSP Ni-Zn ferrite films were then investigated. DC resistivity and loss tangent at microwave frequencies were measured. These films were found to be very absorbing with  $\tan \delta > 10$ . Work performed with Westinghouse internal funds immediately after technical completion of this program showed that this problem is, at least in part, due to a high water content in our films. A procedure, not optimized as yet, for drying the films after growth has yielded significant improvements in the loss factor.

## 2.2 FILM GROWTH PROCESS

The overall SSP process involves three steps: the hydrolysis of an aqueous solution containing ferrous ( $\text{Fe}^{2+}$ ) and other metal ( $\text{M}^{n+}$ ) ions, oxidation, and the ferrite-formation reaction. Successful application of this technique to the deposition of ferrite films can therefore be achieved by understanding the hydration process of specific metal ions in an aqueous solution as a function of pH and concentration. Oxidation is controlled by a proper oxidizing reagent, perhaps with the help of high temperature. The ferrite-formation reaction is controlled by temperature. The solid state properties of the films grown are directly related to these three solution chemistry factors.

Accordingly, detailed tracking and correlation of microstructures and composition, as well as electric and magnetic properties with critical solution factors, were performed during the course of this program.

T. Takada et al.<sup>2</sup> characterized the formation conditions of spinel ferrite in a wet solution as a function of reaction temperature, pH of the reaction solution, and concentration of divalent metal hydroxide,  $\text{Fe}(\text{OH})_2$ . In their study, the pH and temperature ranges required to form spinel ferrites were identified and it was found that  $\text{Fe}_3\text{O}_4$  starts to form above  $40^\circ\text{C}$  at  $\text{pH} \approx 10$ . However, by increasing the temperature, the pH range for the existence of the  $\text{Fe}_3\text{O}_4$  phase increases rapidly covering from 6 to 11 at  $70^\circ\text{C}$ . Although they did not specify the conditions above  $70^\circ\text{C}$ , the data presented indicate that the pH range is wider, covering from 5 to 12 at  $100^\circ\text{C}$ . These conditions were readily adapted to the SSP method.

#### 2.2.1 SSP Apparatus

The SSP apparatus designed and built for this program can be used to deposit ferrite films onto three 3-inch diameter substrates at a time. Figure 5 shows a photograph of the apparatus. Figure 6 is a schematic diagram showing each of its components. Only two of the three nozzles shown were used. Substrates were placed on the substrate holder, which was spun during film deposition to attain film thickness uniformity as well as to wash excessive oxide particles away from the substrate surface. The holder was heated by a heater located underneath it. Substrate temperatures were monitored at the middle of the sample holder's top surface. Reaction and oxidizing solutions, kept at room temperature, were carried from separate containers to their corresponding spray nozzles by means of two Cole-Palmer Masterflex pumps. The spray nozzles were placed directly above the substrates.

The SSP equipment is relatively simple and inexpensive compared with film deposition techniques requiring high vacuum. Furthermore, it could easily be adapted to a production facility requiring deposition onto many substrates or over large surface areas, planar or otherwise.

#### 2.2.2 Film Growth

Although Ni-Zn ferrite films were grown with various chemical compositions of the reaction solution throughout the program, initial

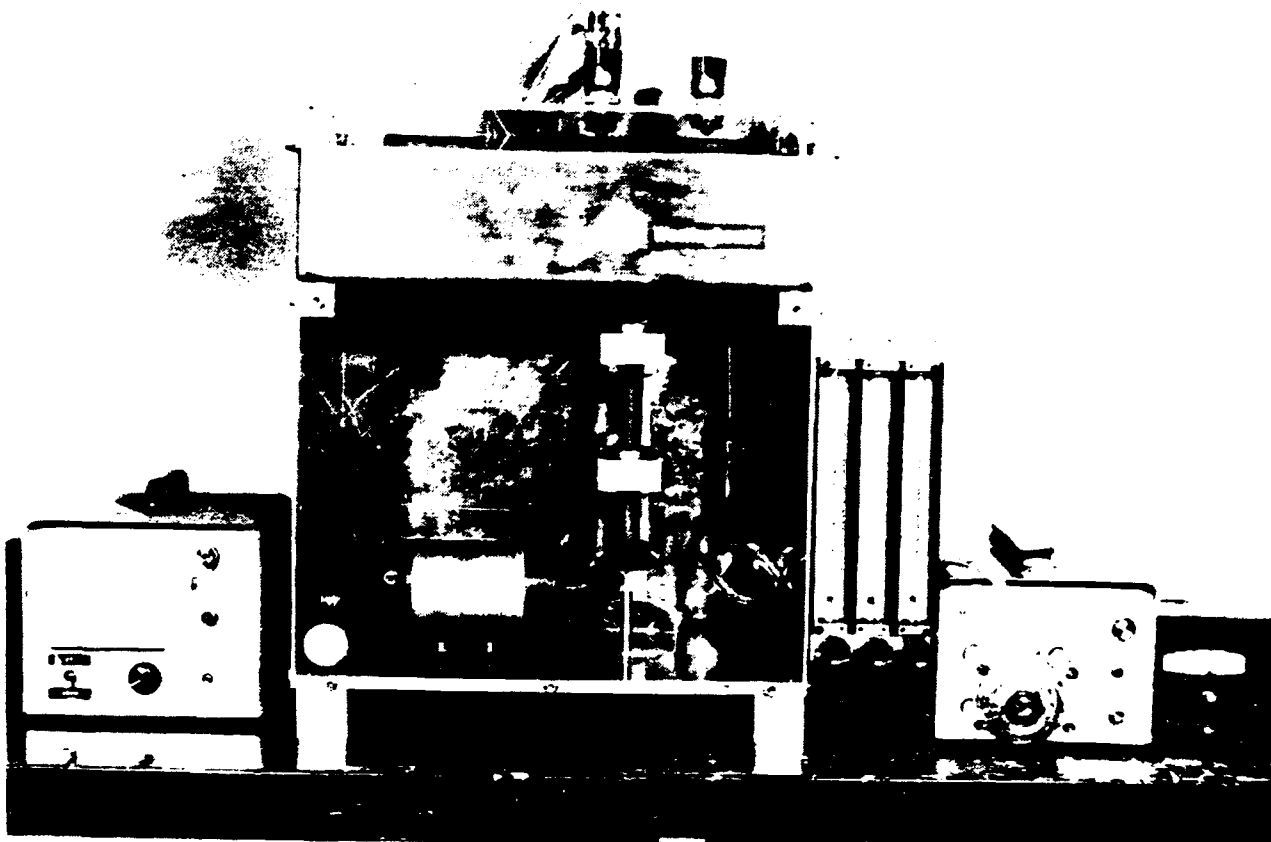


Figure 5. Spin-spray plating (SSP) apparatus.

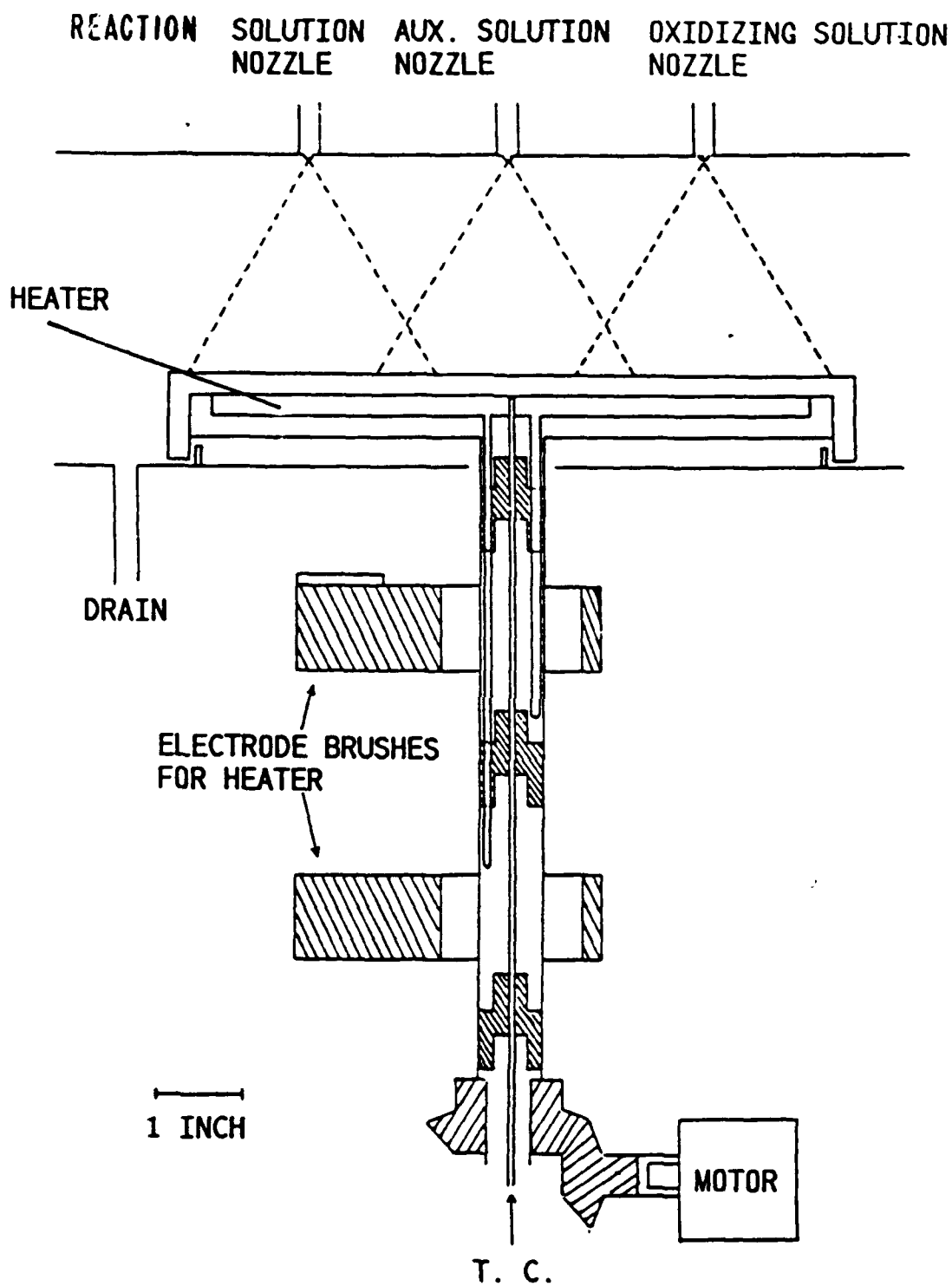


Figure 6. Schematic diagram of the SSP apparatus.

growth experiments were performed at a specific composition, given in grams of the metal chloride per liter of distilled water:  $\text{FeCl}_2$  at 3.0 g/l,  $\text{NiCl}_2$  at 1.5 g/l, and  $\text{ZnCl}_2$  at 0.02 g/l. The distilled water was prepared by bubbling nitrogen gas overnight, prior to addition of the reaction solution chemicals, to eliminate the oxygen gas dissolved in it. The oxidizing solution was prepared also in distilled water from  $\text{NaNO}_2$  at 0.5 g/l and  $\text{CH}_3\text{COONH}_4$  at 5.0 g/l. The pH of each solution was 5.5 and 6.9, respectively.

Although the pH values of each solution were fixed at 5.5 and 6.9, Ni-Zn ferrite films can be grown in a wide range of pH at about  $100^\circ\text{C}$ . Figure 7 is a phase diagram showing the effect of pH and reaction temperature on the formation of various kinds of precipitated phases. As shown in this phase diagram,  $\text{Fe}_3\text{O}_4$  can be formed within the pH range from 6 to 11 at  $70^\circ\text{C}$ . However, the formation of  $\text{Fe}_3\text{O}_4$  is also a function of  $\text{Fe}(\text{OH})_2$  in the solution. In our investigation, it was found that the reaction for  $(\text{Ni}, \text{Zn}, \text{Fe})_3\text{O}_4$  formation can only take place above  $90^\circ\text{C}$  at  $\text{pH} = 5.5$ .

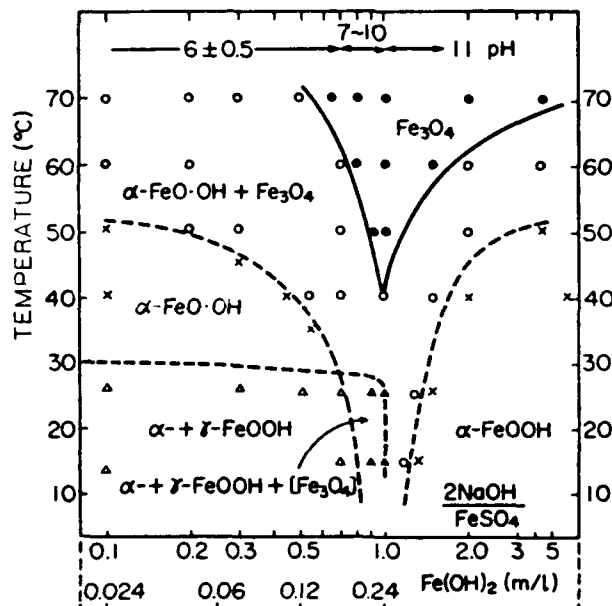


Figure 7. Effect of pH and reaction temperature on the formation of various kinds of precipitates (after reference 2).



Substrate temperature is indeed another important parameter needed to obtain the right ferrite phase,  $(\text{Ni,Zn,Fe})_3\text{O}_4$ . As mentioned in the previous paragraph, it was found experimentally that the reaction of ferrite formation can only take place above  $90^\circ\text{C}$ . This critical reaction temperature was investigated by the following series of simple experiments. Reaction and oxidizing solutions with compositions given above, respectively, were prepared in two separate beakers. Both solutions were heated up to a certain (the same) temperature and then made to react by mixing them together in a third beaker. This was carried out at 60, 85, 95, and  $100^\circ\text{C}$ , respectively. The solutions reacted immediately after mixing, and subsequently ferrite particles were precipitated. These ferrite powder samples were filtered from the solution and examined in our automated Philips X-ray powder diffractometer. The results of this analysis are shown in Figures 8 and 9. As these figures indicate, Ni-Zn ferrite formed only for solution temperatures 95 and  $100^\circ\text{C}$ . At the solution temperatures of 65 and  $85^\circ\text{C}$ , the  $\alpha\text{-FeO(OH)}$  phase is predominant. Based on these results, plating experiments were then performed at temperatures between 90 and  $100^\circ\text{C}$ . The aqueous solutions would evaporate at temperatures above  $100^\circ\text{C}$ .

The surface structure of the films was controlled by the spray pattern of the solutions through the spray nozzles. It was important that the solutions be sprayed uniformly across the substrate surface. The uniformity of spraying was dependent simultaneously on the nozzle design and the distance between the nozzles and the substrates. We originally obtained two nozzles from Professor Abe; however, they did not prove satisfactory in our equipment. After a failed attempt at fabricating nozzles with our own design, we found low-cost units manufactured by Spraying System Co., IL, which were very effective at a given distance from the substrates. This distance had to be readjusted every time the nozzles were replaced.

GaAs, Si,  $\text{Gd}_3\text{Ga}_5\text{O}_{12}$  (GGG), alumina, and glass were used as substrate materials with and without an intermediate layer of gold, which, in principle, would become the ground plane of a potential ferrite device. Substrate temperatures were varied from  $94$  to  $102^\circ\text{C}$ . The spinning rate of the sample holder and the flow rate of the solutions were 50 rpm and 60 ml/min, respectively. The best results were obtained when the growth temperature was held close to  $100^\circ\text{C}$ .

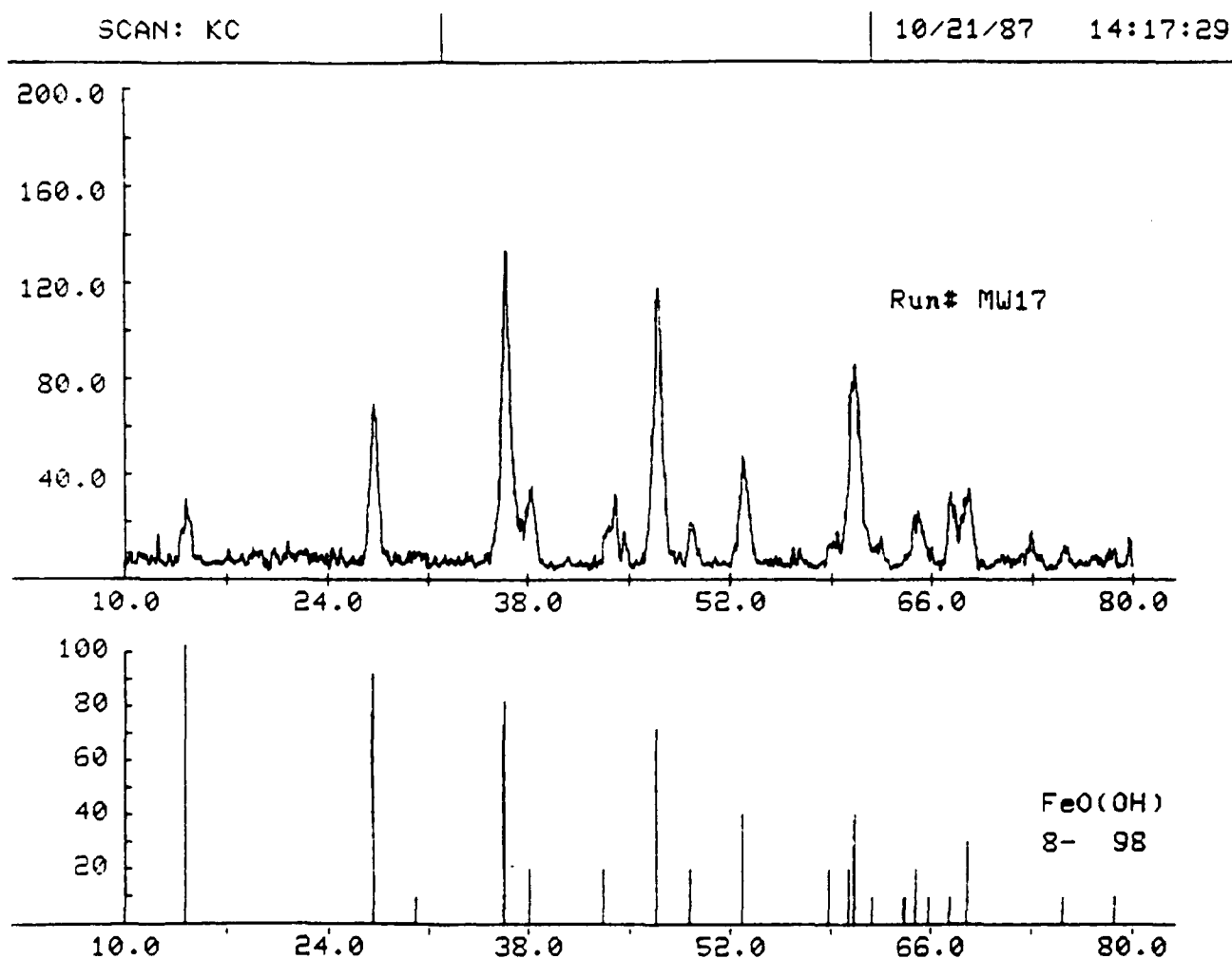


Figure 8. X-ray diffraction pattern of  $\text{FeO(OH)}$  obtained from the precipitated particles in the mixed solution resulting from the reaction and oxidizing solutions at  $60^\circ\text{C}$  and  $85^\circ\text{C}$ .

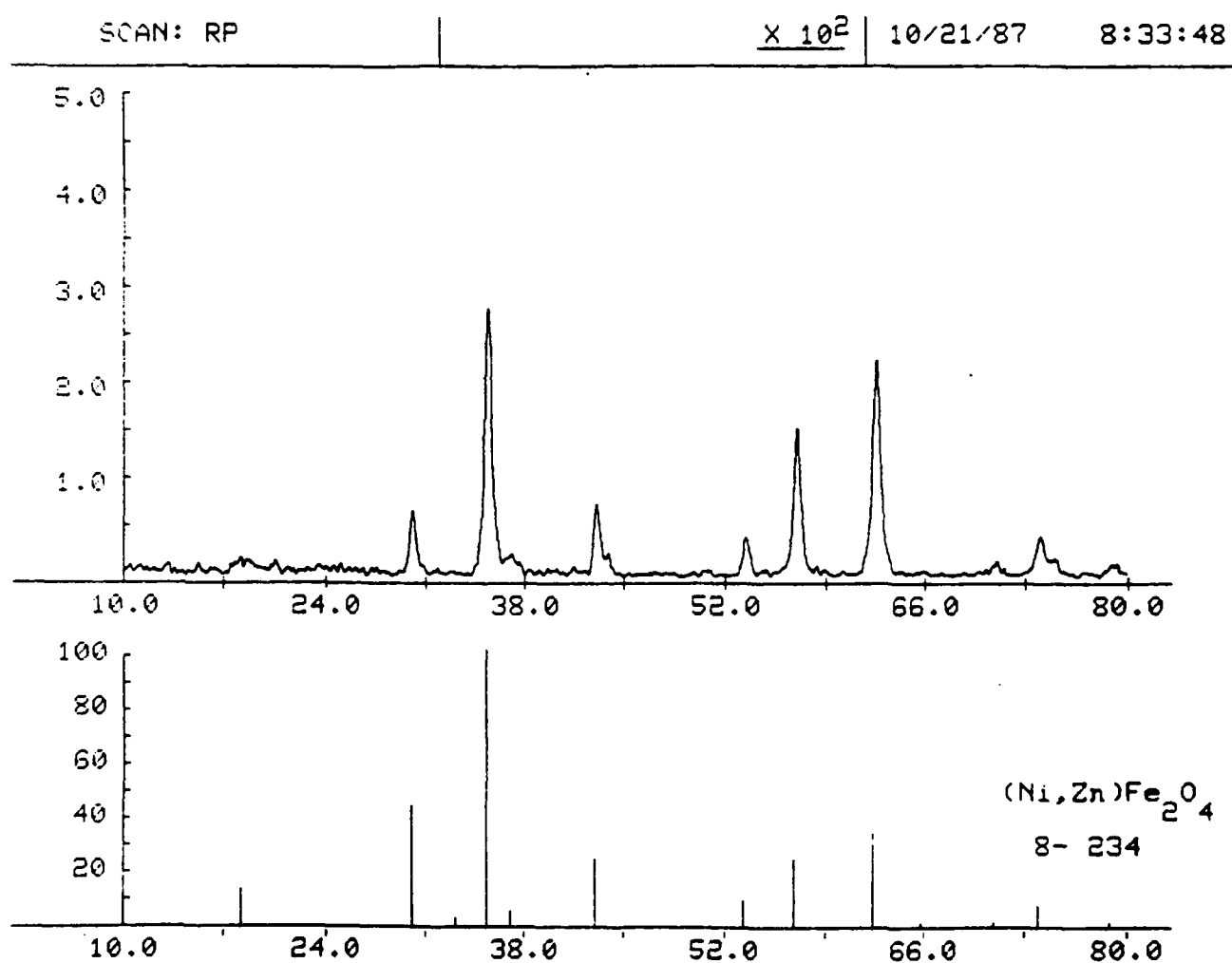


Figure 9. X-ray diffraction pattern of Ni-Zn ferrite obtained from the precipitated particles in the mixed solution resulting from the reaction and oxidizing solutions at 95°C and 100°C.

## 2.3 FILM CHARACTERIZATION

### 2.3.1 Microstructure and Composition

Ni-Zn ferrite films grown onto glass substrates (2-inch by 3-inch) showed three different crystallographic textures depending on the deposition conditions. The (111), (110), and (211) textures predominated at substrate temperatures of 102, 97, and 94°C, respectively. X-ray diffraction patterns for representative sample films showing these textures can be seen in Figure 10. The corresponding plating conditions are given in Table 1. The films were 1.5  $\mu\text{m}$  thick after a deposition time of 1 hour. Film surfaces were very smooth and shiny over most of the film area. A photograph of a typical film surface is shown in Figure 11.

The composition dependence of the lattice parameter was also studied by X-ray diffraction. Three films, MW61, MW63, and MW64, were prepared using different reaction solutions (Table 2). The chemical composition of the films was measured by electron microprobe. In the X-ray diffraction spectra in Figure 12, the position of the (333) reflection peak for each film shifts systematically with chemical compositions. Observed lattice parameters and chemical compositions for these films are shown in Table 3.

Although we prepared these samples using equal amounts of  $\text{FeCl}_2$  and  $\text{NiCl}_2$  in the reaction solutions, the iron and nickel contents in the films varied from sample to sample as the zinc content in the reaction solution ( $\text{ZnCl}_2$ ) was varied (Tables 2 and 3). The reason is that the composition of SSP-grown films is controlled by the compatibility of metal ions with the available spinel lattice sites (tetrahedral or octahedral) under specific chemical equilibrium conditions particular to the SSP process. These conditions are not fully understood as yet. It must be noticed from Table 3 that the Ni and Zn substitution for divalent iron is not complete, and so we do not obtain  $\text{Ni}_x\text{Zn}_{1-x}\text{Fe}_2\text{O}_4$  but, rather,  $\text{Ni}_x\text{Zn}_y\text{Fe}_{2-x-y}\text{O}_4$ . This is an important difference from ceramic samples, which are prepared from a completely different process resulting in greater control of the composition as well as full substitution for the  $\text{Fe}^{2+}$  ions. This is an important consideration in obtaining films with a high electrical resistivity, as will be shown later.

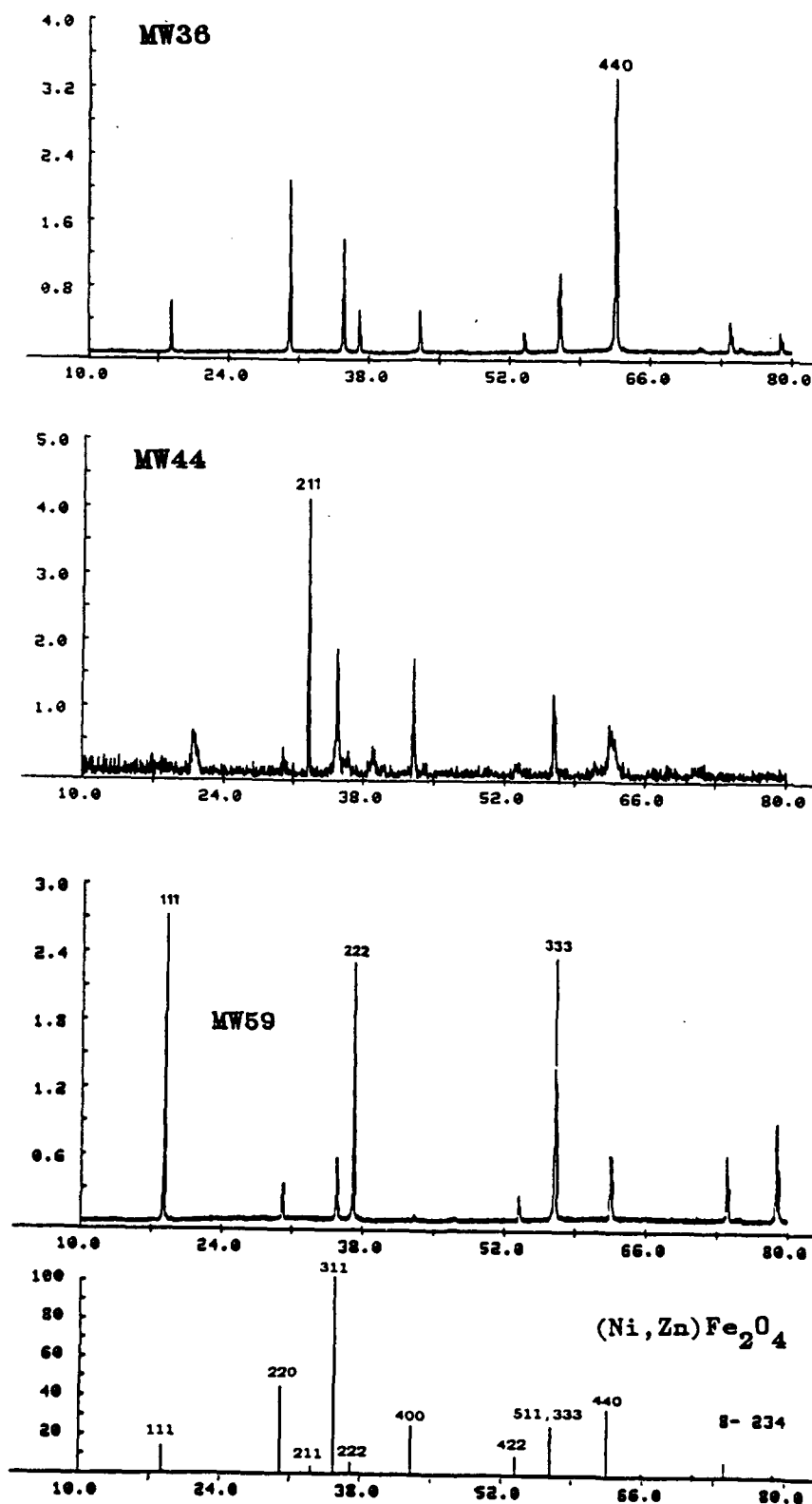


Figure 10. X-ray diffraction patterns for three different films showing the (110), (211), and (111) textured structures. These films were grown with substrate temperatures at 97, 94, and 102°C, respectively.

Table 1

PLATING CONDITIONS UNDER WHICH DIFFERENT  
TEXTURED STRUCTURES WERE OBTAINED

Substrate Used: Glass; Plating Time: 1 hr;  
Film Thickness: Approx. 2  $\mu$ m.

Run No.	Reaction Sol.	Oxidizing Sol.	Sub. Temp.	Spin Rate	Flow Rate	X-ray		
MW36	FeCl <sub>2</sub>	6.0 gm	NaNO <sub>2</sub>	1 gm	97°C	50 ml/min	(110)	
	NiCl <sub>2</sub>	3.0 gm	CH <sub>3</sub> COONH <sub>4</sub>	30 gm			Texture	
	ZnCl <sub>2</sub>	0.04 gm	DI H <sub>2</sub> O	4 l				
	DI H <sub>2</sub> O	4 l						
MW44	FeCl <sub>2</sub>	6.0 gm	NaNO <sub>2</sub>	1 gm	94°C	110 rpm	30 ml/min	(211)
	NiCl <sub>2</sub>	3.0 gm	CH <sub>3</sub> COONH <sub>4</sub>	30 gm				Texture
	ZnCl <sub>2</sub>	0.04 gm	DI H <sub>2</sub> O	4 l				
	DI H <sub>2</sub> O	4 l						
MW59	FeCl <sub>2</sub>	12 gm	NaNO <sub>2</sub>	2 gm	102°C	25 rpm	60 ml/min	(111)
	NiCl <sub>2</sub>	6 gm	CH <sub>3</sub> COONH <sub>4</sub>	20 gm				Texture
	ZnCl <sub>2</sub>	0.08 gm	D.I.H <sub>2</sub> O	4 l				
	DI H <sub>2</sub> O	4 l						



Figure 11. A Ni-Zn ferrite film (2 in. x 3 in.) grown on a glass substrate.

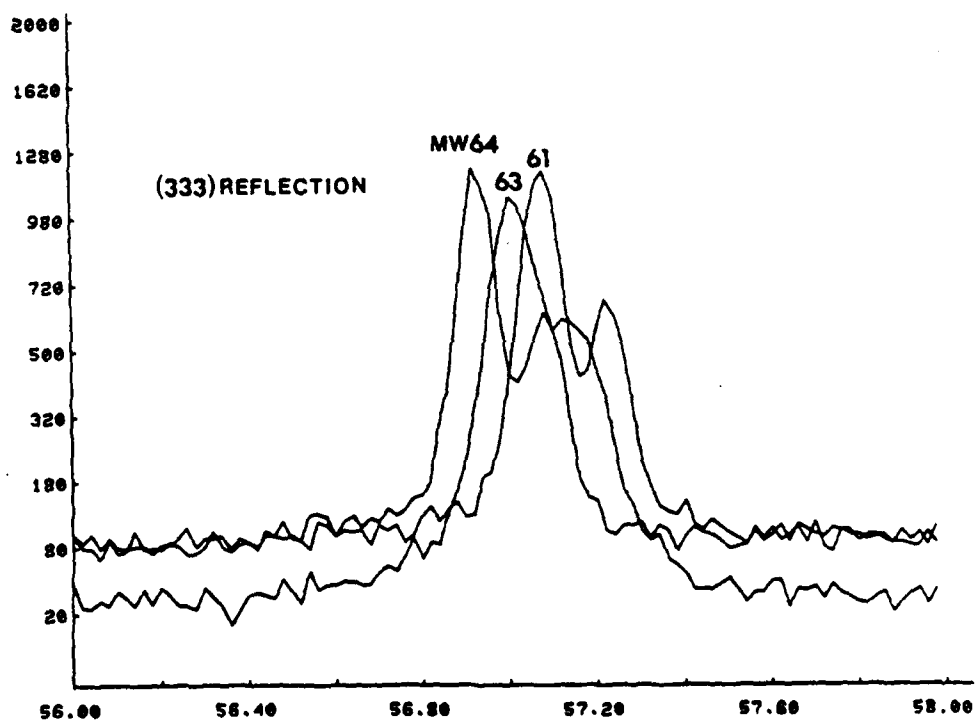


Figure 12. The (333) X-ray reflection spectra for three Ni-Zn ferrite films with compositions listed in Table 2.

Table 2

AQUEOUS SOLUTIONS USED FOR STUDYING THE  
COMPOSITION DEPENDENCE OF THE LATTICE PARAMETER

Sample No.	Reaction Sol.	(gm/l)	pH	Oxidizing Sol.	(gm/l)	pH
MW61	FeCl <sub>2</sub> :	3.0	5.5	NaNO <sub>2</sub> :	0.5	6.9
	NiCl <sub>2</sub> :	1.5		CH <sub>3</sub> COONH <sub>4</sub> :	5.0	
	ZnCl <sub>2</sub> :	0.0				
MW63	FeCl <sub>2</sub> :	3.0	5.5	NaNO <sub>2</sub> :	0.5	6.9
	NiCl <sub>2</sub> :	1.5		CH <sub>3</sub> COONH <sub>4</sub> :	5.0	
	ZnCl <sub>2</sub> :	0.02				
MW64	FeCl <sub>2</sub> :	3.0	5.5	NaNO <sub>2</sub> :	0.5	6.9
	NiCl <sub>2</sub> :	1.5		CH <sub>3</sub> COONH <sub>4</sub> :	5.0	
	ZnCl <sub>2</sub> :	0.04				

Table 3

FILM COMPOSITION AND LATTICE PARAMETERS OF FERRITE  
FILMS GROWN FROM DIFFERENT SOLUTION COMPOSITION

Sample No.	Film Composition	Lattice Parameter (A)
MW61	Ni <sub>0.52</sub> Fe <sub>2.78</sub> O <sub>4</sub>	8.376
MW63	Ni <sub>0.25</sub> Zn <sub>0.12</sub> Fe <sub>2.63</sub> O <sub>4</sub>	8.389
MW64	Ni <sub>0.19</sub> Zn <sub>0.28</sub> Fe <sub>2.53</sub> O <sub>4</sub>	8.397



### 2.3.2 Magnetic Characterisation

Film samples were characterized magnetically using a 9 GHz ferromagnetic resonance (FMR) spectrometer. The apparatus consisted of a resonant cavity made up of a section of rectangular waveguide between a short circuit and an iris which was adjusted for nearly critical coupling. Perturbations in the cavity Q due to the presence of a magnetic sample were detected synchronously, using a lock-in amplifier, by properly modulating the applied bias field. This applied field was swept in the vicinity of a magnetic resonance yielding, at the output of the lock-in amplifier, the derivative of the FMR absorption as a function of applied magnetic field. The samples measured were 2 mm by 2 mm in area. A typical set of measurements for a given sample consisted of observations of the FMR spectra for applied magnetic fields perpendicular and parallel to the plane of the film.

Table 4 summarizes the most salient aspects of the analysis. Some of the films grown showed multiple resonance peaks, indicating a lack of magnetic uniformity. Such lack of uniformity was found in all the films grown on glass which, curiously enough, are the ones that showed a textured structure, as discussed above. Magnetic nonuniformity was also found in a sample taken from the center of a film grown on a 2-inch diameter Si wafer coated with gold, but not in a sample taken out of the edge of the same wafer (Table 4). It was then concluded that in run MW62, an equilibrium temperature was not achieved before growth began, and that while the edges of the wafer did reach a proper growth temperature, the center did not. Each run included both glass and Si substrates, and it was found that in other runs a desired equilibrium temperature was apparently reached for the Si wafers (0.6 mm thick) but not for the thicker (1 mm) glass plates. If the multiple FMR peaks were due to the presence of a phase different from Ni-Zn ferrite, it could not be confirmed by X-ray diffraction, which showed only a single phase for each of these films. Figure 13 shows the perpendicular FMR spectra for run MW62 on gold-on-Si for samples at the edge and the center of the wafer, respectively. In these traces the sample from the wafer center gives a multiple resonance, whereas that at the wafer edge gives a single, clean resonance, although there is a slight hint of nonuniformity, perhaps indicating that the proper growth temperature was barely reached in this area of the wafer.

Table 4

## SUMMARY OF FMR CHARACTERIZATION

Growth Conditions: Temperature:  $\sim 100^\circ\text{C}$ ;  
Spin Rate: 25 rpm; Flow Rate: 60 ml/min.

Run No.	Substrate	Composition	$4\pi M_s$ (G)	$\gamma$ (GHz/kOe)	$\Delta H_\perp$ (Oe)	$\Delta H_\parallel$ (Oe)
MW61	Au/Si	Ni <sub>0.22</sub> Zn <sub>0.00</sub> Fe <sub>2.78</sub> O <sub>4</sub>	5228	2.992	121	277
	Glass		*	-	-	-
MW62	Au/Si (edge)	Ni <sub>0.25</sub> Zn <sub>0.12</sub> Fe <sub>2.63</sub> O <sub>4</sub>	5462	3.062	312	330
	Au/Si (center)		-	-	-	-
	Glass		-	-	-	-
MW64	Au/Si	Ni <sub>0.19</sub> Zn <sub>0.28</sub> Fe <sub>2.53</sub> O <sub>4</sub>	4790	3.124	121	172
	Glass		-	-	-	-

\*Where no magnetic data are given, multiple perpendicular resonances were observed. The reasons for these are as yet unknown.

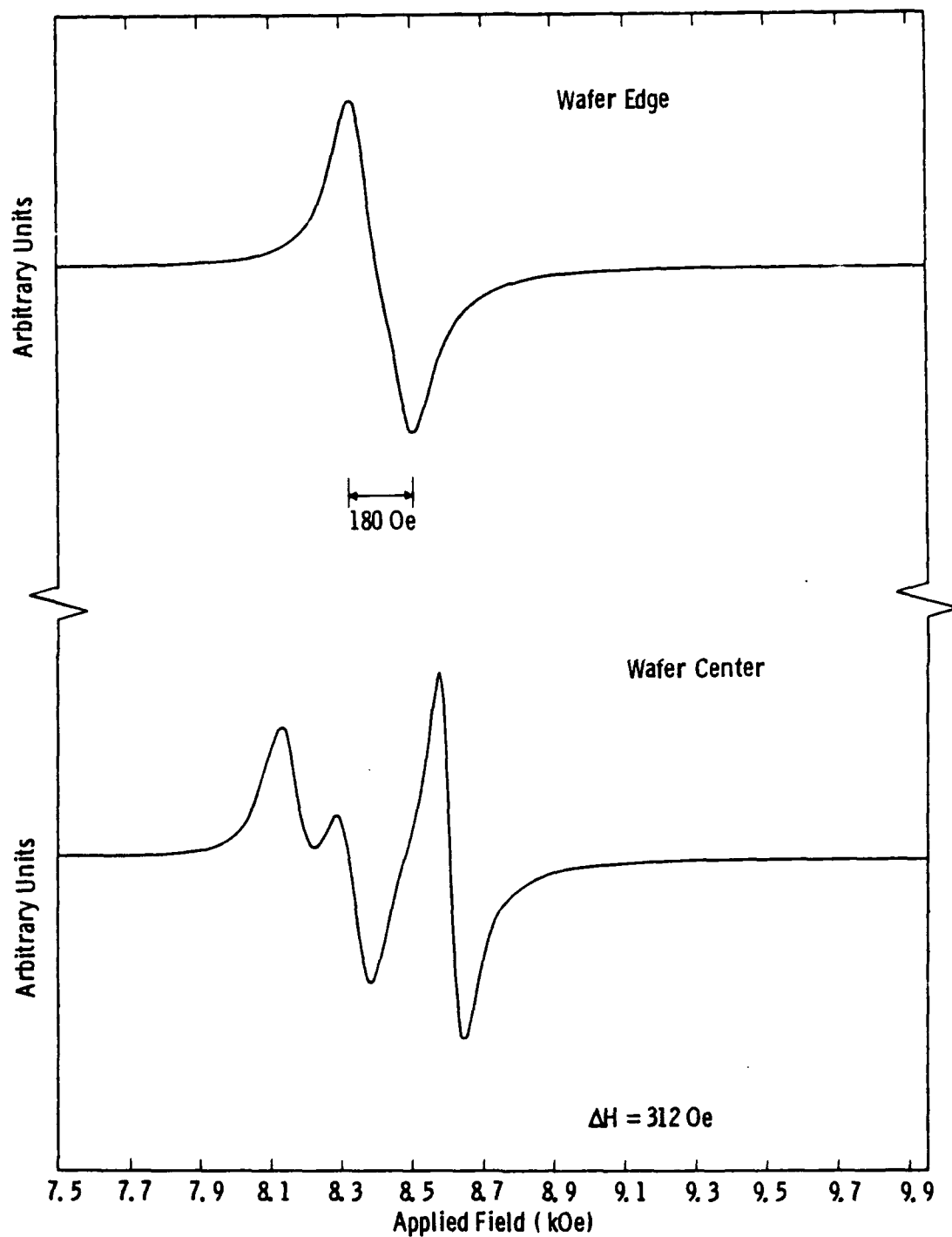


Figure 13. Perpendicular FMR spectra for samples from a) the wafer edge and b) the wafer center of film MW62 on gold-on-silicon.

The effect of Zn content on the film's magnetic properties is also given in Table 4. FMR analysis yielded saturation magnetization values for these samples which seem to agree with published results<sup>3</sup> on the correlation between Zn content in spinel ferrites and  $4\pi M_s$ . Thus, the saturation magnetization increases to 5.5 KG for  $x = 0.12$  and then diminishes gradually with further increase in Zn content.

The ferromagnetic resonance linewidths obtained vary from sample to sample, with that for the parallel resonance being in many cases significantly wider than that for perpendicular resonance. This is to be expected for samples which show a lack of magnetic perfection. These imperfections cause coupling to spin waves which are degenerate with the lowest order magnetostatic-wave mode in the sample for parallel bias field, thus broadening the resonance linewidth. The perpendicular resonance linewidth, on the other hand, can be considered as close to the minimum achievable, and in two of our films reached as low as 83 Oe, which compares very favorably with commercially available polycrystalline material. One of these two samples was grown on a GaAs wafer and will be discussed below. The linewidths obtained are, on the whole, comparable to those published in the literature.<sup>3</sup>

The gyromagnetic ratios, calculated from the resonance data, are consistently around 3 GHz/KOe, varying from 2.94 to 3.24 GHz/KOe depending on the sample, which also compares well with published values<sup>3</sup> and commercial samples.<sup>4</sup>

Our best and most significant result, from the perspective of microwave device fabrication, was a rather thick film (4  $\mu\text{m}$ ) grown on evaporated gold on a GaAs wafer. The parallel and perpendicular resonance curves are shown in Figure 14, which shows that the perpendicular linewidth was only 83 Oe. This film was grown in two hours at a high growth rate. From the FMR data,  $4\pi M_s = 5620$  G and  $\gamma = 3.0$  GHz/KOe. The parallel resonance linewidth was 260 Oe, more than three times higher than the perpendicular resonance linewidth.

## 2.4 FILMS FOR DEVICE STRUCTURES

Fabrication of practical microstrip microwave and millimeter-wave magnetic devices requires that the ferrite material be sandwiched between a ground plane and a top-surface metallization to be patterned.

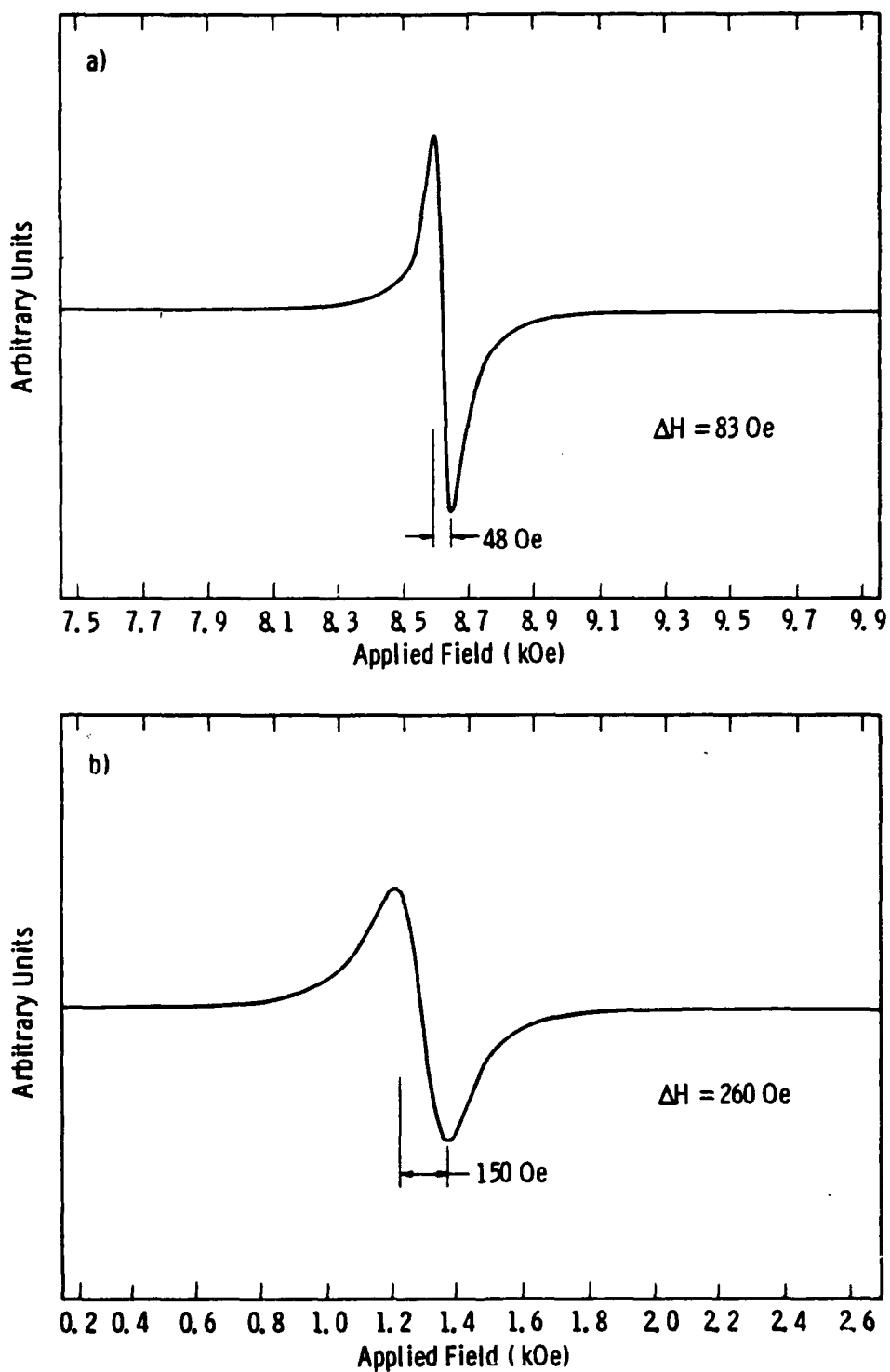


Figure 14. a) Perpendicular and b) parallel FMR data for sample MW63 ( $4 \mu\text{m}$ ) on gold-on-GaAs. From these curves,  $\gamma = 3.0 \text{ GHz/KOe}$ ,  $4\pi M_s = 5820 \text{ G}$ .

In addition, to minimize conductor and dielectric losses, the ferrite films must be as thick as possible, i.e., greater than 100  $\mu\text{m}$ , the thinnest GaAs typically handled for power devices. In principle, then, it was established that SSP ferrite films must be deposited onto GaAs substrates coated with a layer of gold electroplated to a typical thickness of about 5  $\mu\text{m}$ . A thin layer of an adhesion promoter, such as  $\text{SiO}_2$ , on the gold was also considered. The adhesion of SSP ferrite films to different substrates and, in particular, to the desired substrate combination was studied in connection with achieving the right thickness.

#### 2.4.1 Thick Film Growth

Initially, most of our SSP films started to peel off from the substrate when the deposition time exceeded 2 to 3 hours. Careful examination of these films indicated they consisted of ultrafine wet powders which are adsorbed on the substrate surface. These wet powders were seen to require a hardening process for proper film thickness build-up. The maximum film thickness that could be grown continuously was determined to be about 3-4  $\mu\text{m}$ . Drying the films overnight at room temperature after each 1- or 2-hour long deposition made it possible to build up the thickness of these films by growing again on the dry films. Successive depositions were performed with this intermediate drying process, so that eventually a 25- $\mu\text{m}$ -thick film was demonstrated (Figure 17).

Multiple-deposition ferrite films were initially prepared on GaAs, Si, and GGG wafers both with and without an intermediate layer of gold on these substrates. These films were grown in four separate steps. The growth conditions for each step were identical: substrate temperature, 95°C, and deposition time of each step, 1 hour. The measured film thicknesses were all about 7  $\mu\text{m}$  after a total deposition time of 4 hours. These results also indicated that the growth rate of ferrite films onto these substrates was higher than on glass substrates.

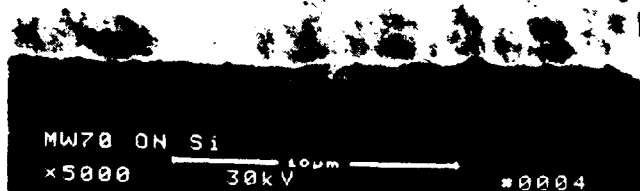
Cross-section views of these films were examined by scanning electron microscope (SEM) and are shown in Figure 15. The films grew with a columnar structure normal to the substrate. X-ray diffraction measurements indicated that, despite their structure, these films exhibit no preferred crystallographic orientation.



These films were grown four times.  
Each deposition time was one hour.  
Substrate Temp.: 95°C  
Spin Rate: 50 rpm  
Flow Rate: 60 ml/min



← Electrodeposited Au  
← Evaporated Au  
← GaAs Substrate



← Electrodeposited Au  
← Evaporated Au  
← Si Substrate



← Gadolinium Gallium  
Garnet (GGG) Substrate

Figure 15. SEM observation of the cross section of Ni-Zn ferrite films grown on GaAs, Si, and GGG.

Growth of thicker films was attempted on GaAs and Si at a substrate temperature of 100°C. A film on GaAs was grown in four separate depositions for a total of 8 hours. An SEM photograph of the cross-sectional structure of this film is shown in Figure 16, where a thickness of about 14  $\mu\text{m}$  can be seen. A film on Si was grown in eight separate depositions for a total of 16 hours, yielding a thickness of about 25  $\mu\text{m}$ . Figure 17 is an SEM photograph of its cross-sectional structure, where some of the constituent layers are clearly visible. This is probably not desirable, since it appears as evidence of small differences between the layers. Figures 18 and 19 show results of X-ray and FMR analyses on this film, respectively. Its crystallographic texture structure (Figure 18) was clearly (111). Compare this figure with Figure 10 (bottom), corresponding to the (111) texture structure of a single layer. The FMR study (Figure 19) shows, however, the different layers that make up this film, which appeared to have slightly different compositions resulting in multiple resonances at different fields.

These experiments demonstrate that the growth of thick films by multiple depositions suitable for practical microwave devices is quite feasible. Tighter control of the growth conditions appears to be required so that the resulting film has uniform characteristics through its thickness. Room temperature drying of each layer seemed adequate although, as will be discussed later, a more sophisticated process may be required to obtain material with low microwave losses.

#### 2.4.2 Film-Substrate Adhesion Studies

Adhesion of ferrite films to the substrate surface was studied by preparing several different surface conditions. Our films generally showed strong adhesion to glass substrates. This is because the glass surface consists inherently of a hydrophilic group,  $-\text{OH}$ , that provides adsorption sites for the metal ions, initiating the ferrite formation. Using Si wafer substrates, ferrite films were grown onto intermediate layers of  $\text{SiO}_2$ , gold, and on a bare Si surface (Figure 20). These films were grown in the same experiment at 97°C for 3 hours; their thicknesses were all about 4.7  $\mu\text{m}$ . During growth, the film on bare Si peeled off in some areas, seen on the photograph as a lighter color. In the other two cases, adhesion was good except over a relatively small area



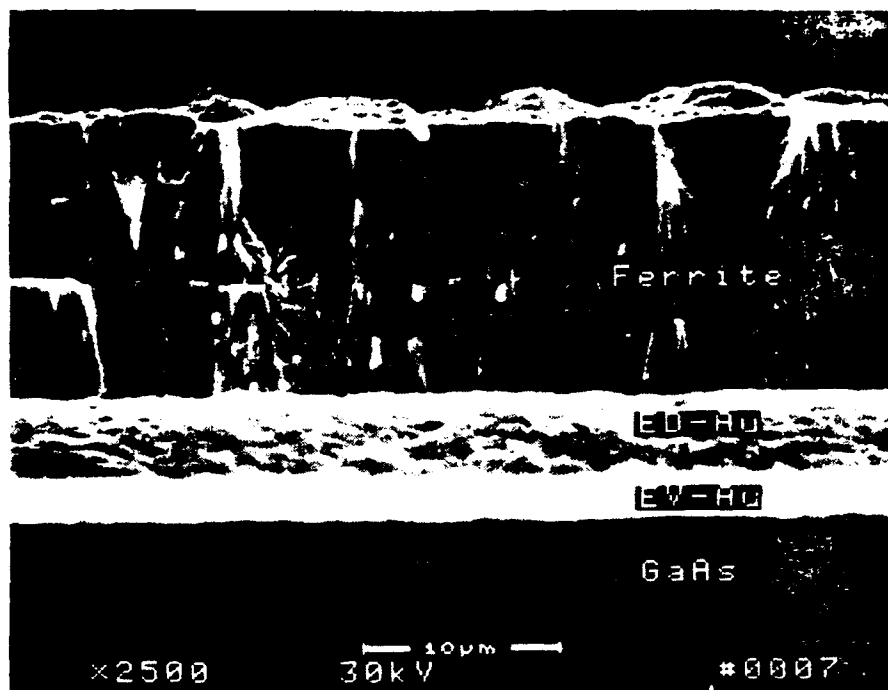


Figure 16. SEM photograph of the cross section of a multilayer Ni-Zn ferrite film on a gold-plated GaAs wafer. The film was grown in four separate depositions for a total of 8 hours. Its thickness is about 14  $\mu\text{m}$ .



Figure 17. SEM photograph of the cross section of a multilayer Ni-Zn ferrite film on a gold-plated Si wafer. The film was grown in eight separate depositions for a total of 16 hours. Its thickness is about 25  $\mu\text{m}$ .

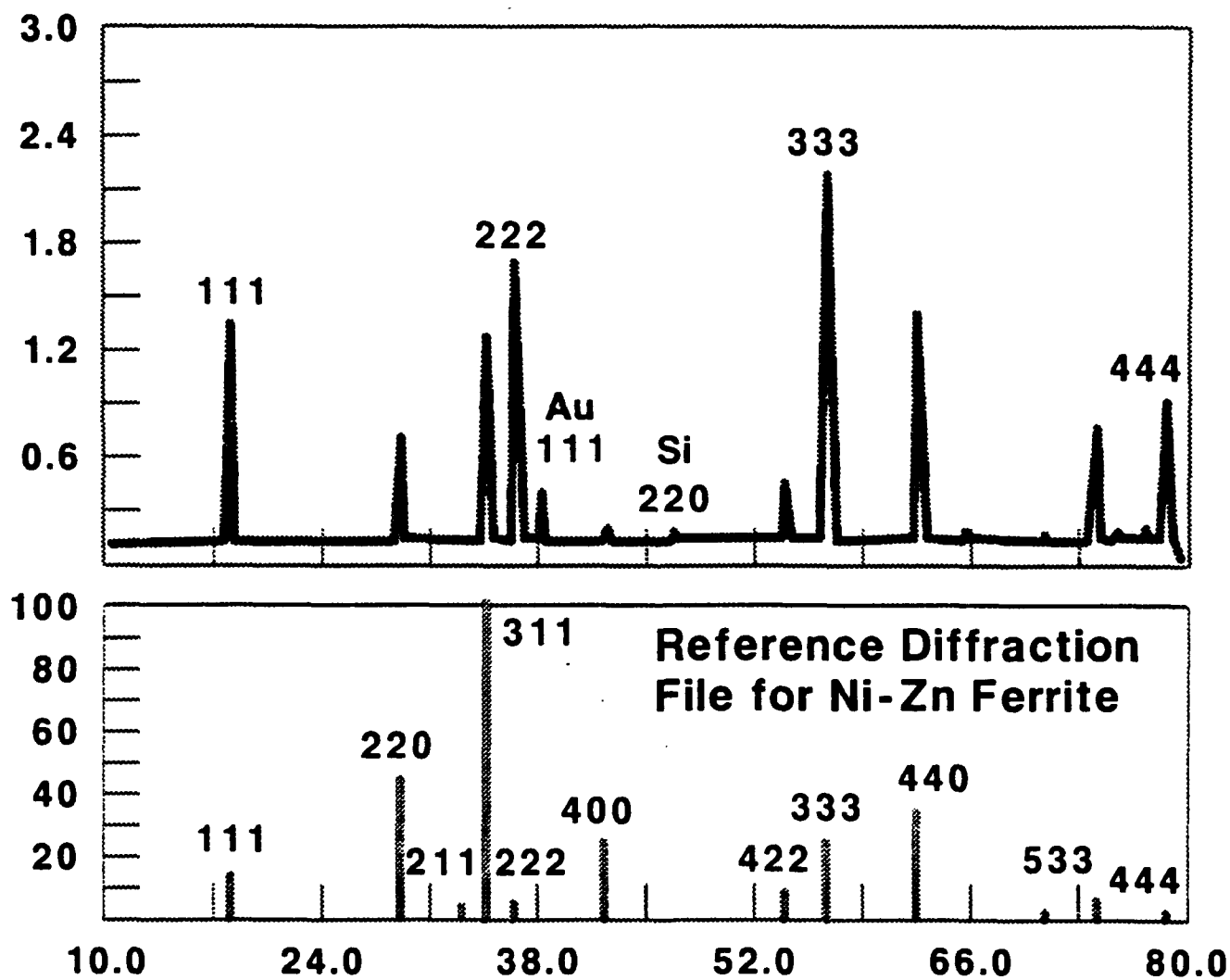


Figure 18. X-Ray diffraction pattern for multilayer 25- $\mu\text{m}$ -thick Ni-Zn ferrite film on Au/Si, showing (111) textured structure.

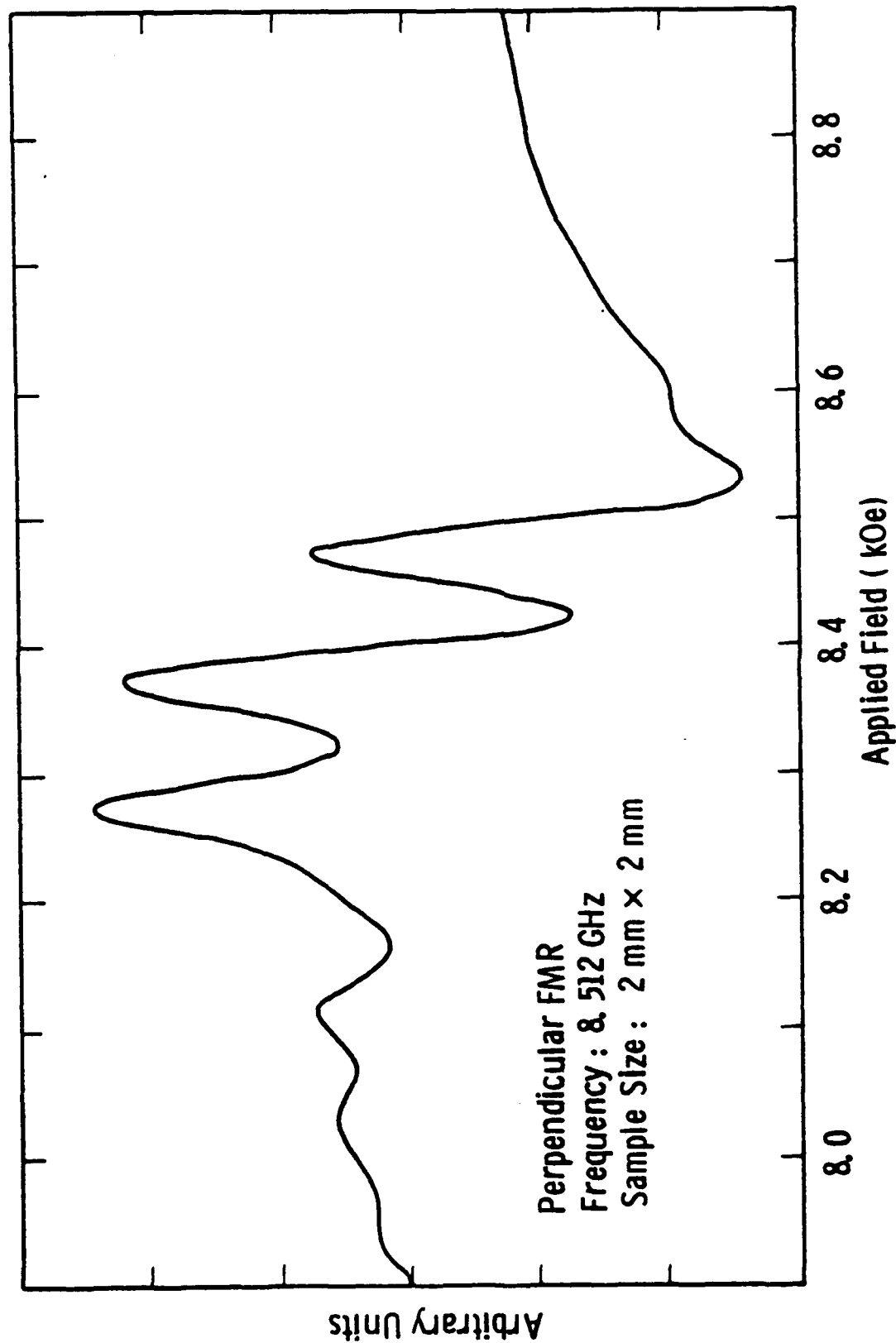


Figure 19. Perpendicular FMR spectrum for 25- $\mu$ m-thick multilayer Ni-Zn ferrite film on Au/Si. Multiple resonance peaks evidence small compositional nonuniformities among different layers.

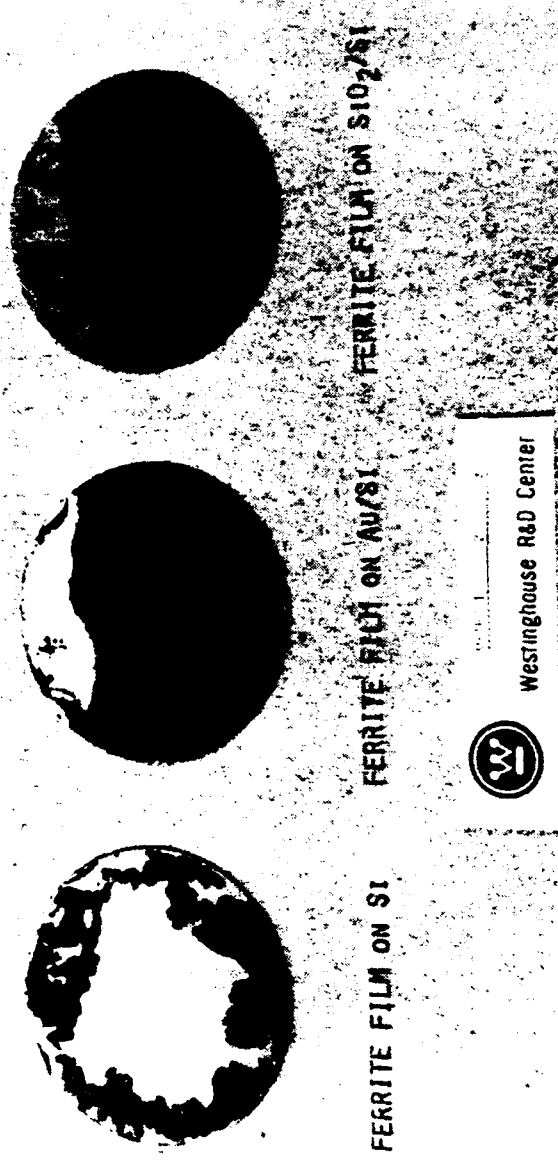


Figure 20. Ferrite films deposited at 97°C and grown on Si, on Au/Si, and on SiO<sub>2</sub>/Si.

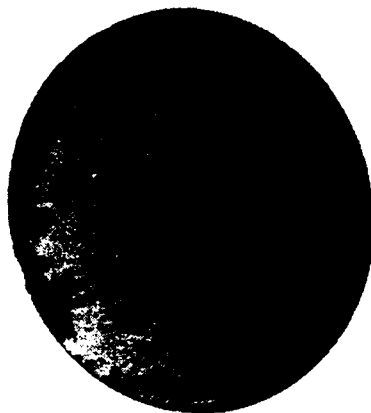
(Figure 20). This appeared to be due to an excessive solution accumulation between the two screws used for holding the samples.

Similar results were obtained from a shorter run (2.5 hours) under the same conditions, using only a bare Si substrate and one with  $\text{SiO}_2$  on Si. These films are about  $3.7 \mu\text{m}$  thick and are shown in Figure 21. In this experiment, most of the ferrite films grown on bare Si peeled off during the plating process, but not so in the case of  $\text{SiO}_2$  on Si. Thus, we conclude from these experiments that films of good quality showing good adhesion can be grown on gold and  $\text{SiO}_2$  layers up to a thickness of about  $3 \mu\text{m}$ . Thicker films can only be grown by the multiple deposition process with the intermediate drying described in the previous section.

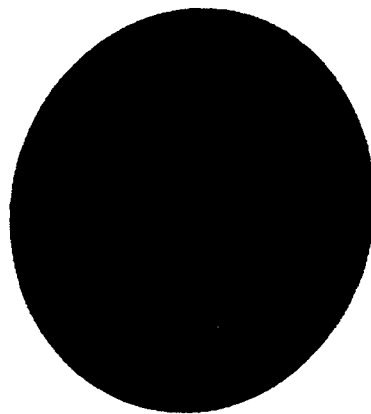
#### 2.4.3 Monolithic Integration of GaAs MMIC's with Ferrite Devices

To fabricate good-performance ferrite devices which also are monolithically integrated with GaAs MMICs, it would be necessary that a ferrite region be sandwiched between a ground plane and a patterned top-surface metallization. This must be so at least for the most common case of microstrip configurations. In order to avoid significant discontinuities which could degrade the characteristics of the ferrite device, the simplest solution is to etch away a portion of the GaAs and put in its place ferrite material. In Figure 22 the processing steps involved in doing this are described schematically. The fourth step, planarization, could be accomplished in a variety of ways which we believe are not necessary to discuss here. It must be also pointed out that the same final configuration could be arrived at by etching from the back of the substrate and depositing the ferrite also from the back, leaving the top, device-quality surface free for later electronic device fabrication.

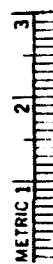
The critical question for us to address here, since it has already been demonstrated that thick films are possible, is whether SSP ferrite films can grow uniformly on a sloping surface. To this end, depressions 2 mm wide (junction circulator at 20 GHz) and 50 to  $100 \mu\text{m}$  deep were prepared by chemical etching on a GaAs wafer and used as the substrate for a SSP deposition run. Since the nature of the experiment did not require that we optimize the procedure to etch the depressions



FERRITE-FILM ON SI



FERRITE-FILM ON  $\text{SiO}_2/\text{Si}$



Westinghouse R&D Center

Figure 21. Ferrite films from a shorter deposition run (2.5 hrs) under the same conditions as Figure 20, but only on bare Si and on  $\text{SiO}_2/\text{Si}$ .

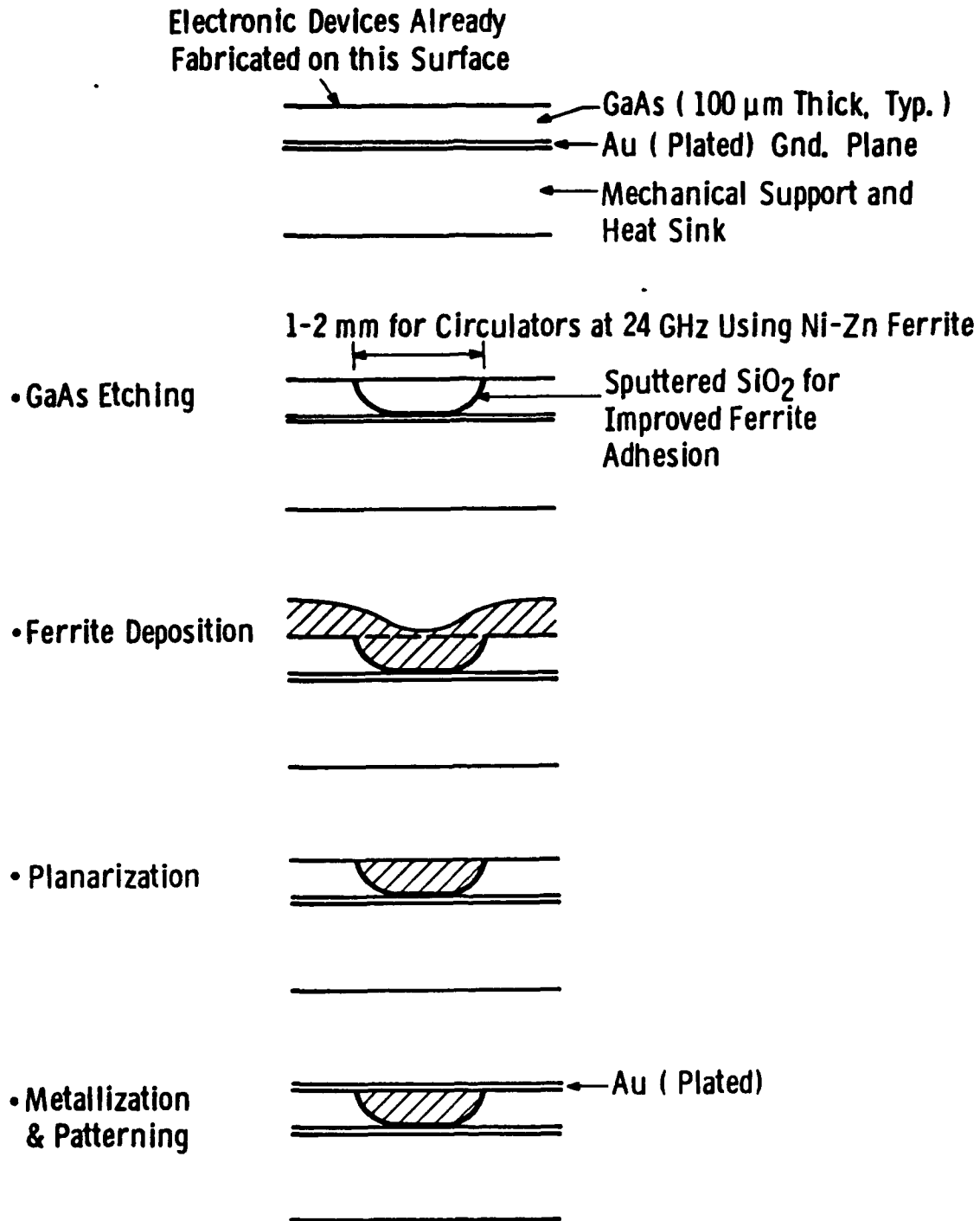


Figure 22. Monolithic integration of microwave magnetic and GaAs devices using spin-spray-plated ferrite films.

in the GaAs, deep and narrow etchpits were inadvertently created as well. The resulting coated wafer was studied under SEM; sample SEM views comprise Figure 23, which shows a depression and numerous etchpits, and Figures 24(a) and (b). The latter two photographs show very clearly that the SSP process is quite suitable for the growth of uniform ferrite films on fairly steep walls. As can be seen in Figure 24(b), the presence of the etchpits turned out to be very useful in determining the capabilities of SSP for coating non-planar regions of a wafer.

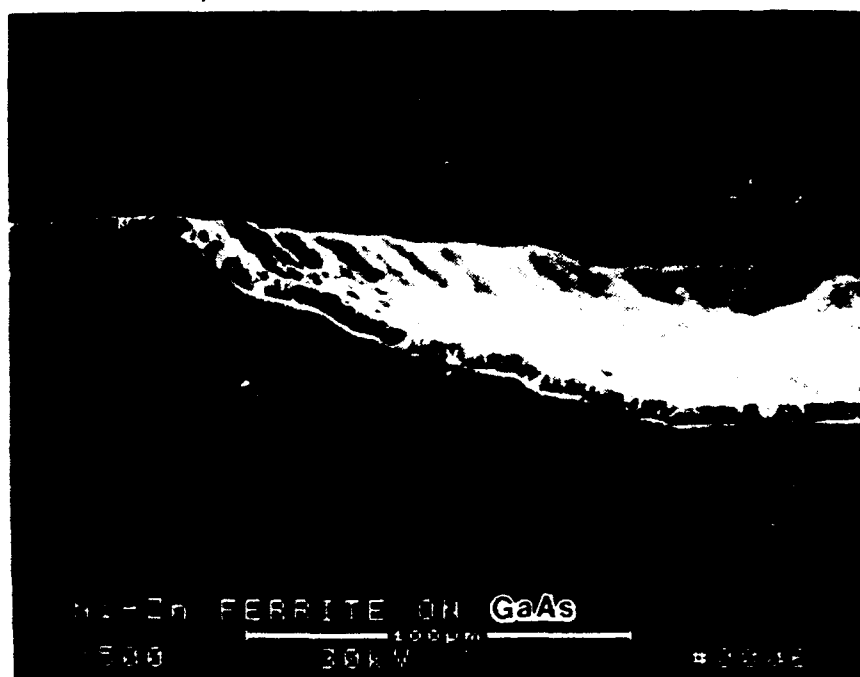
It must be pointed out that the configuration proposed above does not include the bias magnet, which perhaps would have to be external to the MMIC structure and added once the monolithic fabrication is completed. An alternative approach is being pursued by Professor F. J. Cadieu, Queens College, NY, under contract from the U. S. Air Force (RADC, Hanscom AFB). It consists of deposition by sputtering of suitable magnetic materials to allow fabrication of the biasing magnet in a monolithic fashion as well.



Figure 23. SEM photograph showing etched cavity and pits on a test GaAs wafer used for an experiment of film deposition on nonplanar geometries.



(a)



(b)



Figure 24. Ni-Zn ferrite film on (a) sloping wall of etched cavity on a GaAs wafer and (b) on steep walls of an etchpit.

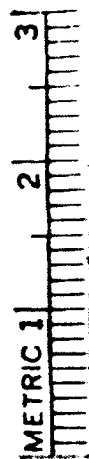
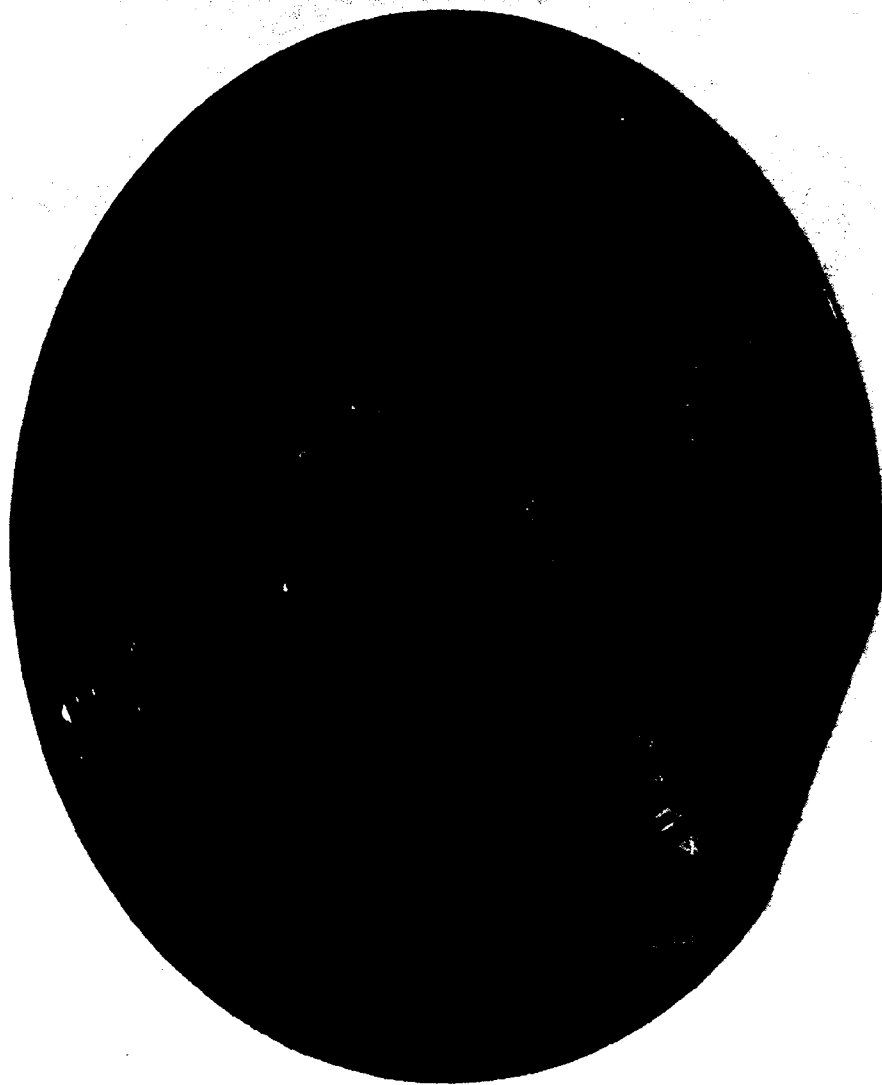
#### 2.4.4 GaAs MMIC Compatibility Experiment

To determine the compatibility of the SSP process with fabricated GaAs monolithic devices, a Ni-Zn ferrite film was deposited on a portion of a GaAs wafer with several MMIC circuits on it. Disks the size of practical circulators at 20 GHz (see Figure 3) were subsequently defined photolithographically on the ferrite film. A test GaAs transistor was measured before and after ferrite deposition and processing to determine if damage was caused to the GaAs devices.

Figure 25 is a photograph of the wafer portion used, which was mounted with photoresist on a 3-inch diameter sapphire wafer for mechanical support. The photograph includes the final ferrite disks, clearly visible at both ends of the GaAs piece. The piece used was a portion of a 3-inch GaAs wafer which had three previously fabricated Wafer Scale T/R modules,<sup>5</sup> each of which included a test P-FET transistor. Figure 26 is a photograph of the entire fabricated wafer showing 16 T/R modules. Figure 27 is the layout of one module showing the location of the P-FET.

First, the GaAs wafer was covered with a thick coating of photoresist, enough to ensure and protection of all the electronic devices. The disks on both ends of the GaAs piece were then defined and the resist developed so that the disk areas were opened up to direct exposure to the ferrite spray. Three ferrite layers were grown to reproduce conditions required to deposit a thick ferrite film suitable for a practical circulator.

Measurements on the test P-FETs in each T/R module, before and after the ferrite film was deposited and patterned, were used to establish if the GaAs devices were damaged. Figures 28(a) and (b) show the results of these measurements, before and after the ferrite processing, respectively, in the form of a wafer map indicating the maximum available gain (MAG) for the P-FET in each module. The difference between the two sets of measurements is believed to be caused by parasitics due to residual photoresist in the areas between the gates and the source and drain. The MAGs, after the ferrite processing, increased steadily as we gradually removed the residual photoresist by repeated ashing. However, it was not possible to remove it completely as shown in the photograph of Figure 29. An optimized process with the proper choice of resist would eliminate this difficulty. The MAG differences before and after



Westinghouse R&D Center



Figure 25. Photograph of GaAs Wafer Scale piece with three T/R modules showing two ferrite disks from deposited and patterned SSP ferrite multilayer films. The disks' diameter is that of a junction circulator of conventional design at 20 GHz. The wafer piece was mounted on a 3-inch diameter sapphire wafer for support.

The remaining process steps include wafer thinning, via formation, via metallization, and via isolation. The present backside processing includes via mask delineation using an infrared aligner, laser drilling/chemical etching for forming the vias, and gold-plating techniques for low via resistance. The processing steps for isolating the signal feedthrough vias (from the backside ground plane) are under development and consist of photoresist delineation of the areas to be isolated, and etching of the backside metal.

The wafer is now completely processed and can be functionally RF tested using the Cascade prober. Figure 3 is a photograph of a fabricated wafer showing 16 T/R cells, while Figure 4 shows a single cell. Figures 5 and 6 show cross-section drawings of the various components needed to form the circuits.

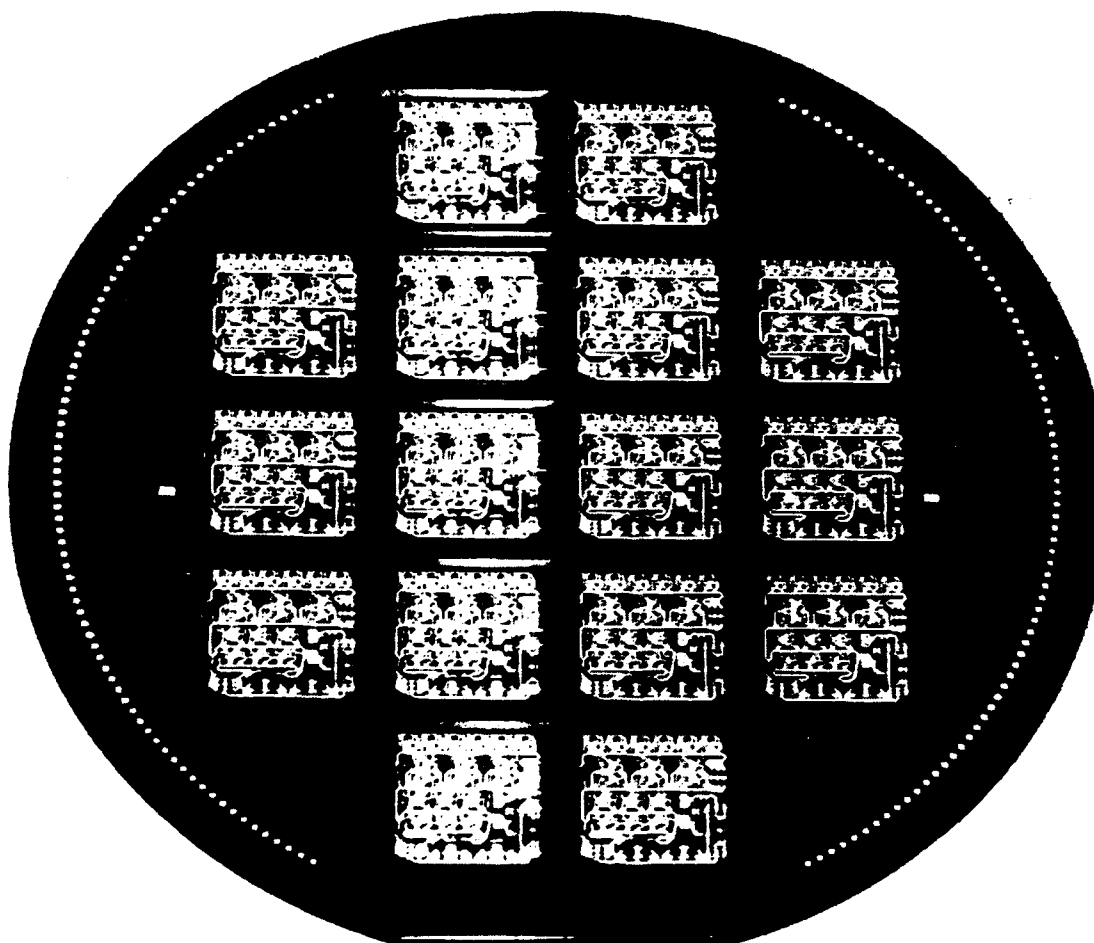


Figure 26. Photograph of fabricated wafer showing 16 T/R cells.

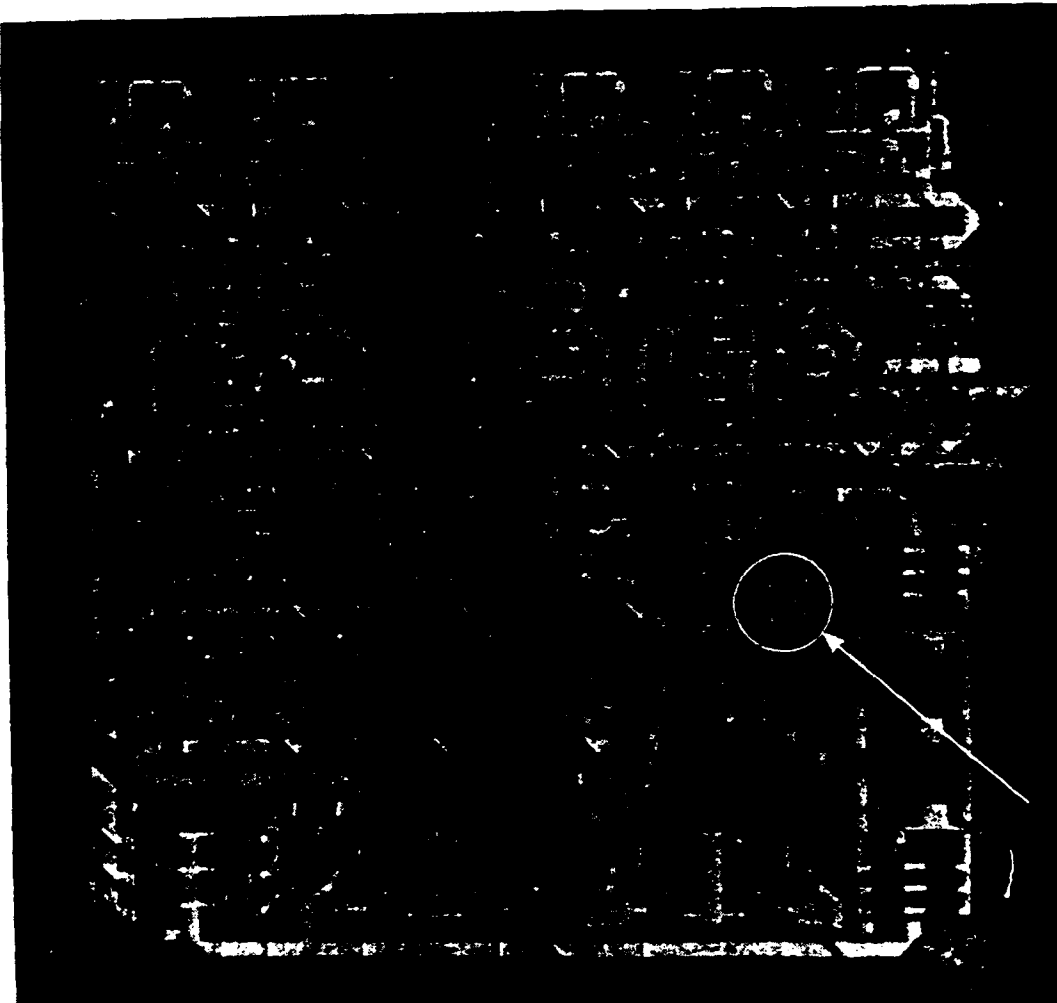


Figure 27. Single cell from a 16 T/R cell wafer.

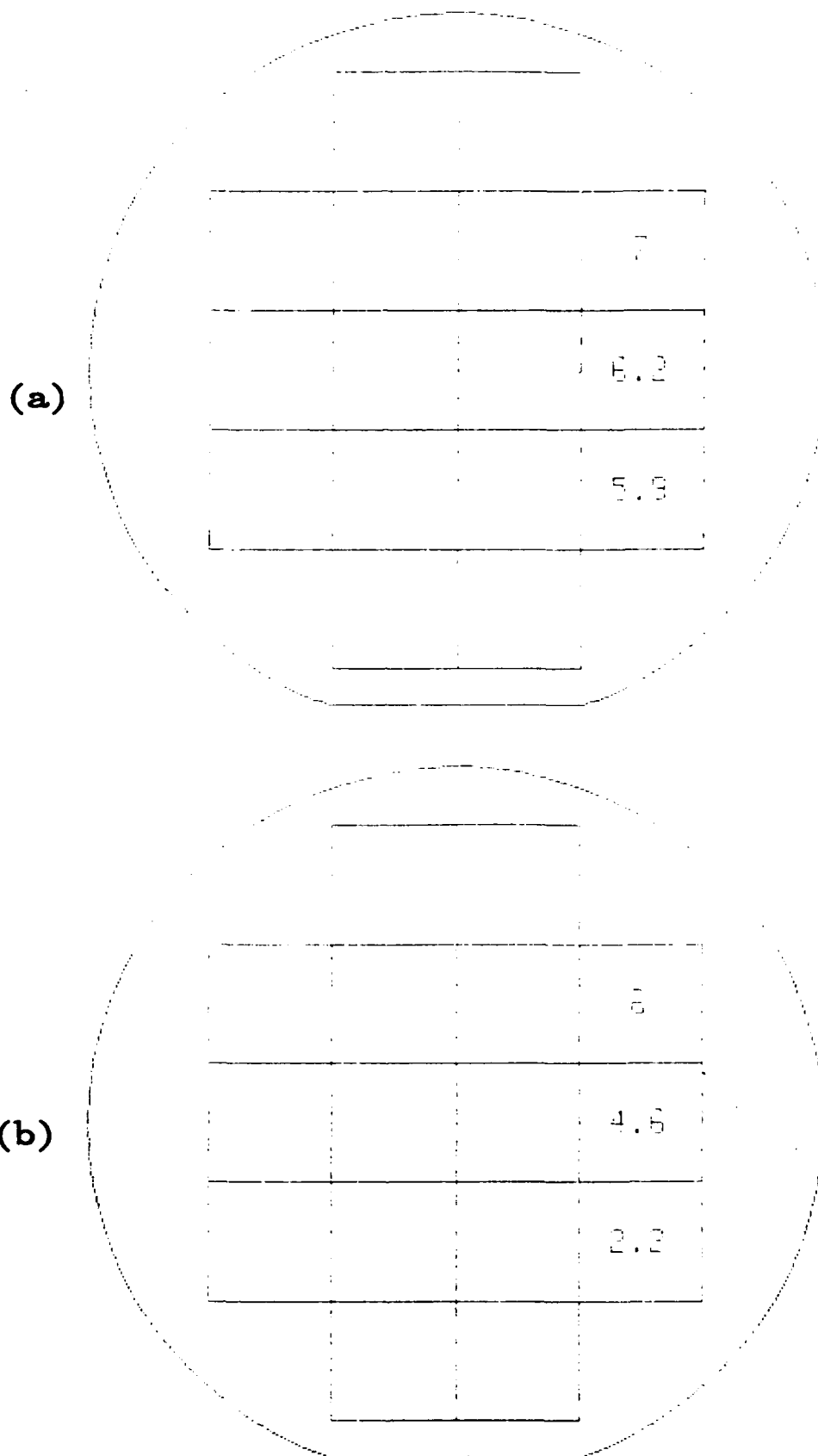


Figure 28. Wafer map of maximum available gain (MAG) for the test P-FETs in each of the three T/R modules shown in Figure 25:  
 (a) before and (b) after ferrite processing. Measurement parameters are indicated in the wafer maps.



Figure 29. 1,000X magnification of the gate areas of one of the test P-FETs showing residual photoresist between the gates and source and drain, thus degrading the transistor performance.

ferrite processing, nevertheless, were felt to be small enough for us to conclude that the experiment was successful. Had the ferrite deposition damaged the transistors, the measurements would have reflected this independently of the residual resist on the gate areas.

## 2.5 ELECTRICAL CHARACTERISTICS

Low-loss microwave magnetic devices require that the materials have dielectric loss tangent ( $\tan \delta$ ) on the order of 0.001 or lower, and dc resistivities greater than  $10^7 \Omega\text{-cm}$ . Ni-Zn ferrite films studied in this program had electrical resistivities ranging from  $10$  to  $10^6 \Omega\text{-cm}$ , depending on the chemical composition of the films.

Low resistivity in Ni-Zn ferrite films is due to the coexisting of ferrous and ferric ions in the octahedral sites of the spinel lat-

tice. This ionic distribution can result in a transfer of electrons between  $\text{Fe}^{2+}$  and  $\text{Fe}^{3+}$  without changing the charge-valency state.

The spinel structure is a cubic structure with a unit cell of 32 oxygen ions.<sup>6</sup> In this cubic close-packed structure, two kinds of interstitial sites exist: the tetrahedral and the octahedral sites, which are surrounded by four and six oxygen ions, respectively. Ferrite structures of this kind could be of the following spinel types:

- Normal spinel structure (e.g.,  $\text{ZnFe}_2\text{O}_4$ ), in which the divalent metal ions occupy the tetrahedral sites and the trivalent ions occupy the octahedral sites.
- Inverted spinel structure (e.g.,  $\text{NiFe}_2\text{O}_4$ ), in which the divalent metal ions occupy some octahedral sites, while the trivalent ions occupy the remaining octahedral sites and all the tetrahedral sites.
- A mixed spinel structure (e.g.,  $\text{Ni}_{1-x}\text{Zn}_x\text{Fe}_2\text{O}_4$ ).

The general cation distribution of spinel ferrites can then be expressed as:

$$\left\{ \text{M}_{\delta}^{2+} \text{Fe}_{1-\delta}^{3+} \right\} \left[ \text{M}_{1-\delta}^{2+} \text{Fe}_{1+\delta}^{3+} \right] \text{O}_4 \quad (1)$$

where

$\{ \}$  tetrahedral sites, with  $\text{M}^{2+}$  being, e.g.,  $\text{Zn}^{2+}$  and  $\text{Mn}^{2+}$ .

$[ \ ]$  octahedral sites, with  $\text{M}^{2+}$  being, e.g.,  $\text{Ni}^{2+}$  and  $\text{Fe}^{2+}$ .

and

$\delta = 1$ , normal spinel distribution

$\delta = 0$ , inverse spinel distribution

$0 < \delta < 1$ , mixed distribution.

Thus, when high electrical resistivity of Ni-Zn ferrite is desired, the existence of  $\text{Fe}^{2+}$  in the octahedral sites has to be suppressed. This can be achieved by increasing the amount of  $\text{Ni}^{2+}$  ions, which would prevent  $\text{Fe}^{2+}$  ions from otherwise occupying the octahedral sites.



The electrical resistivity of spinel ferrites is dependent on their chemical composition, i.e., substitution of a specific cation can modify the site distribution of other ions in the spinel lattice, resulting in changes in electrical resistivity. In the case of ferrites produced by SSP, however, since this is an equilibrium chemical process, the control of film compositions is limited by an incompatibility of desirable transition metal ions with the tetrahedral and octahedral cation sites.

In the present investigation, our goal was to study the growth conditions required to obtain a specific chemical composition yielding high electrical resistivity and, as a consequence, low microwave losses. As will be seen, however, even though relatively large resistivities were obtained ( $10^6 \Omega\text{-cm}$ ), they did not completely correlate with film compositions measured, for reasons not yet understood.

#### 2.5.1 Electrical Resistivity Measurements

DC electrical resistivity measurements were made by the two-point probe method using an electrometer and a probe contact arrangement inside a shielded dry box. A photograph showing the experimental set-up inside the dry box is shown in Figure 30. The samples were held in place by means of a vacuum chuck. A small soldering iron, visible in the photograph, was used to heat up one of the contact pads and measure the thermoelectric voltage to determine the type of conduction observed. Gold contacts were evaporated on the ferrite film surface. The gap between each pair of contacts was  $1,000 \mu\text{m}$  wide by  $50 \mu\text{m}$  long so fringing field effects could be neglected. An array of several pairs of contacts were deposited on each sample to obtain a suitable average measurement over the surface area of the sample. Three 3-cm by 2-cm samples were cut from each 5-cm by 7.5-cm film measured. Small variations were observed across the surface of most of the samples measured, attributable, perhaps, to small thickness nonuniformities. Figure 31 is a photograph of a sample with 15 pairs of gold contacts.

Figure 32 shows a typical I-V characteristic for one of the samples grown. The resulting resistivity was confirmed by van der Pauw measurements, also indicated in the figure. This curve corresponds to a sample with one of the highest resistivities measured (see Figure 33).

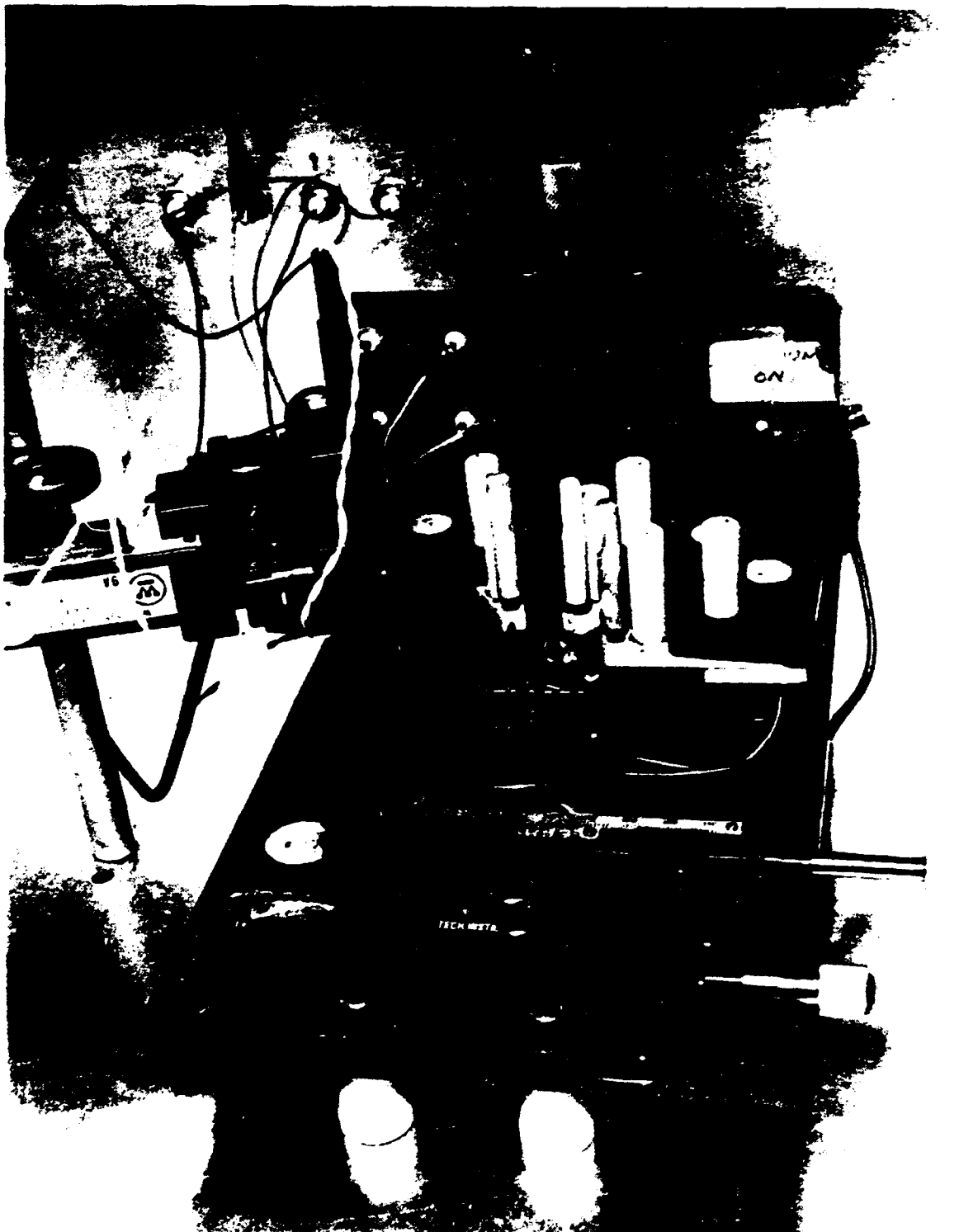


Figure 30. Photograph of two-point probe dc resistivity measurement equipment.

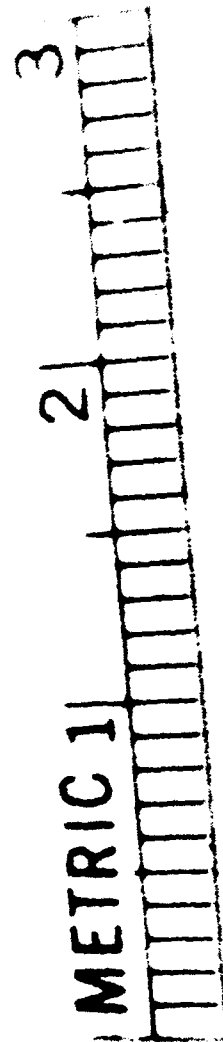
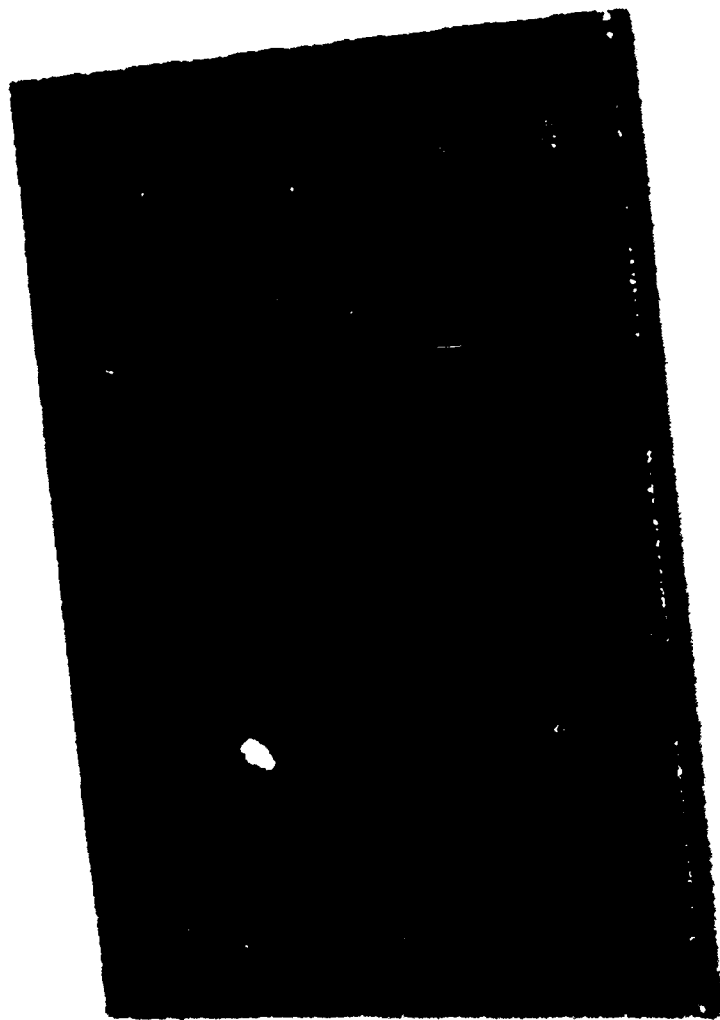


Figure 31. Photograph of sample with 15 pairs of gold contacts for dc resistivity measurements.

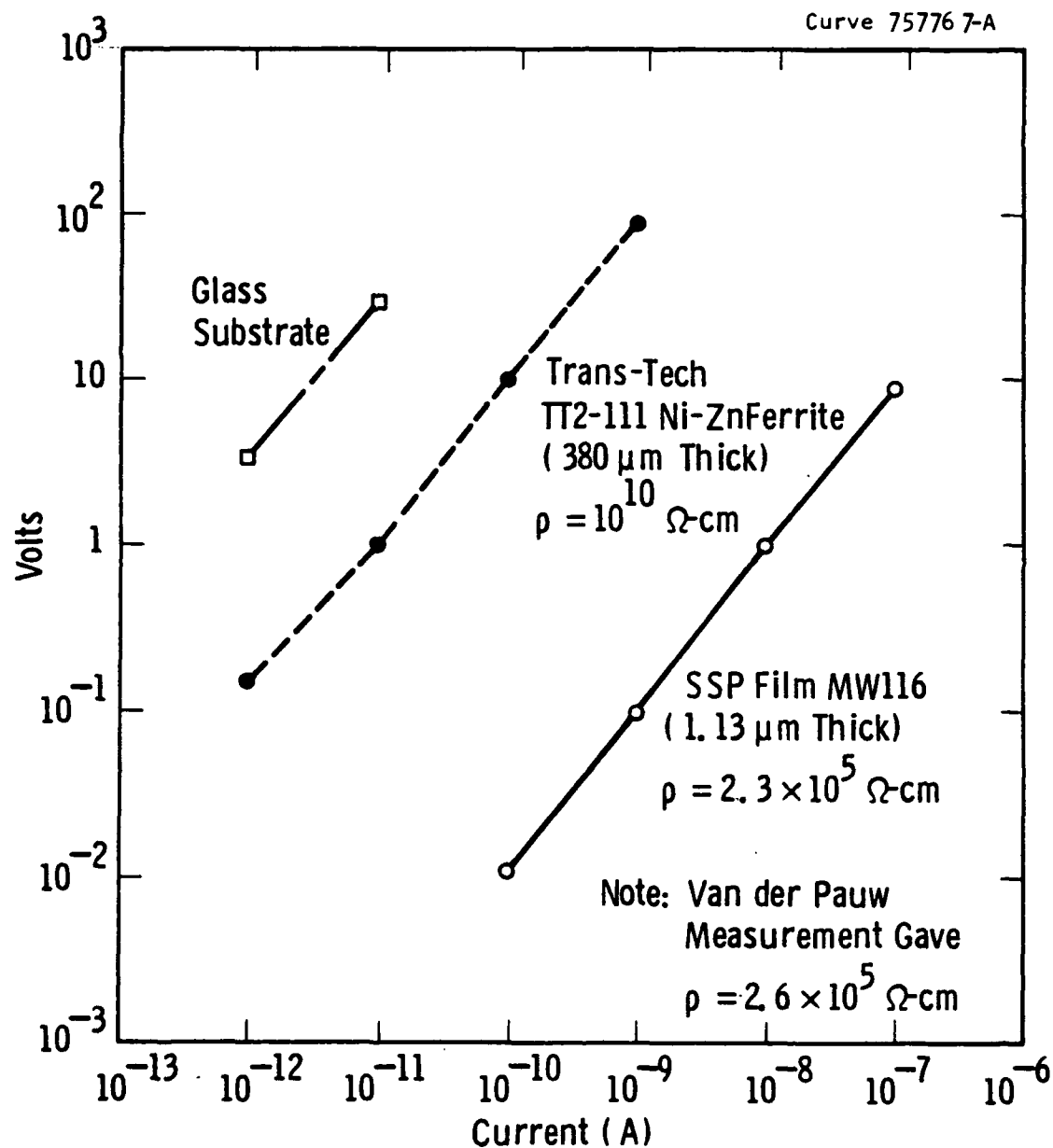


Figure 32. Comparison of V-I characteristics for Ni-Zn ferrite film MW116 with those for a commercial sample and the glass substrate MW116 was grown on.

I-V curves for all the other samples tested were equally linear. Included in Figure 32, for comparison, are the I-V curves of the glass substrate and a commercially available ceramic sample.<sup>4</sup>

The thermoelectric voltage was also measured for several samples by applying heat to the grounded contact pad. In all cases a positive voltage was measured, indicating n-type conduction.

Figure 33 is a bar-graph showing the wide range of resistivities measured. The composition dependence of the dc electrical resistivity was investigated for five of the films prepared from different compositions of the reaction solution, as shown in Table 5. Table 6 shows the results of resistivity measurements and the film compositions analyzed by electron microprobe. Although we prepared all the samples using the same amount of  $\text{FeCl}_2$  in the reaction solution, the iron content varied from sample to sample. Samples MW99, MW100, MW111, and MW113 were also prepared using the same amount of  $\text{NiCl}_2$  in the reaction solution; however, their Ni contents appeared different from each other. These results imply that the film composition is not strongly dependent on the solution composition. Rather, as mentioned before, the composition is controlled by an incompatibility of transition metal ions with spinel lattice sites under specific chemical equilibrium conditions particular to the SSP process. The end result is that the iron content in the samples grown for this study exceeded the desired stoichiometric ratio expressed by the general formula  $\text{MFe}_2\text{O}_4$ , that is,  $(\text{Ni}+\text{Zn}+\text{Mn}):\text{Fe} = 1:2$ . Instead, what we have been able to grow so far has the general formula:



Nevertheless, the electrical resistivities of these samples varied over five orders of magnitude, i.e., from 8 to  $10^6 \, \Omega\text{-cm}$  (Figure 33). Table 6 shows what seems to be a lack of correlation between the iron content in a sample and its resistivity. Thus, MW99 appears to be richer in iron than MW100 and yet has a somewhat smaller resistivity. MW111, on the other hand, has almost the same iron content as MW99 and a resistivity four orders of magnitude lower. We were unable to explain the variation in resistivity with composition from our limited experimental data. We

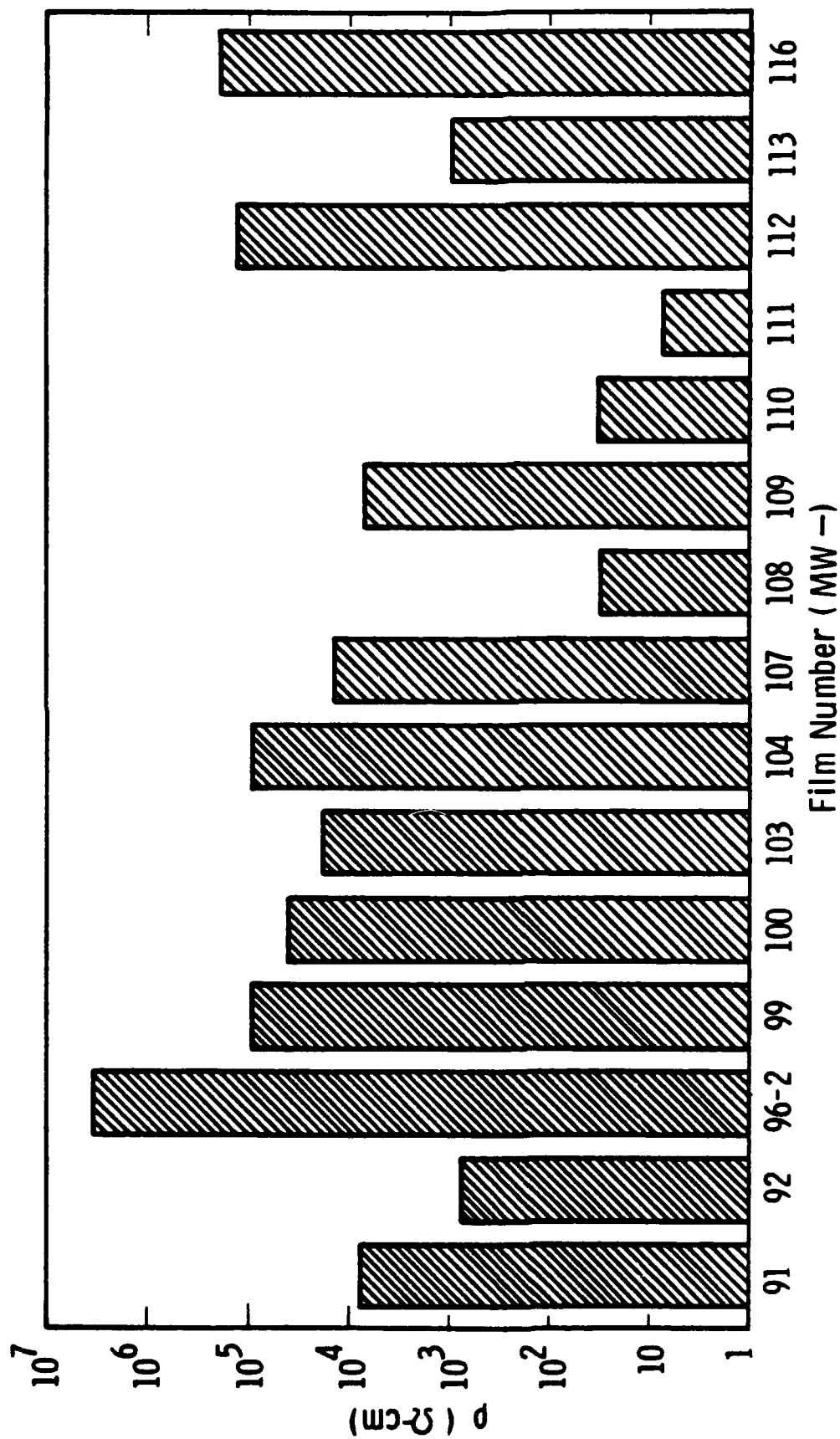


Figure 33. Bar-graph of maximum resistivities ( $\Omega\text{-cm}$ ) for SSP films measured.

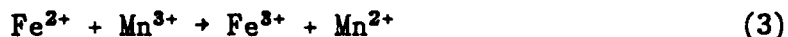
Table 5  
SOLUTION COMPOSITIONS

Sample	Reaction Solution (gm/l)				Oxidizing Solution (gm/l)	
	FeCl <sub>2</sub>	NiCl <sub>2</sub>	ZnCl <sub>2</sub>	MnCl <sub>2</sub>	NaNO <sub>2</sub>	CH <sub>3</sub> COONH <sub>4</sub>
MW99	3	1.5	0.02	-	0.5	5
MW100	3	1.5	0.04	-	0.5	5
MW111	3	1.5	-	0.02	0.5	5
MW113	3	1.5	0.02	0.02	0.5	5
MW116	3	2.5	0.04	-	0.5	5

Table 6  
CHEMICAL COMPOSITION AND ELECTRICAL RESISTIVITY

Sample	Chemical Composition	Resistivity ( $\Omega$ -cm)
MW99	Ni <sub>0.12</sub> Zn <sub>0.25</sub> Fe <sub>2.63</sub> O <sub>4</sub>	10 <sup>4</sup>
MW100	Ni <sub>0.4</sub> Zn <sub>0.21</sub> Fe <sub>2.39</sub> O <sub>4</sub>	4.4x10 <sup>4</sup>
MW111	Ni <sub>0.4</sub> Mn <sub>0.0008</sub> Fe <sub>2.6</sub> O <sub>4</sub>	8
MW113	Ni <sub>0.24</sub> Zn <sub>0.12</sub> MnO <sub>0.00013</sub> Fe <sub>2.57</sub> O <sub>4</sub>	1.2x10 <sup>3</sup>
MW116	Ni <sub>0.3</sub> Zn <sub>0.24</sub> Fe <sub>2.46</sub> O <sub>4</sub>	4x10 <sup>5</sup>

know that the addition of small amounts of manganese in ceramic ferrites can increase electrical resistivity<sup>7</sup> because the concentration of  $\text{Fe}^{2+}$  can be kept low by the  $\text{Mn}^{3+}$  ions as described by the relation:



Samples MW111 and MW113 were prepared using a reaction solution containing Mn. However, as Table 6 shows, the film composition analyses indicated very small amounts of Mn in them.

In conclusion, we were unable to learn sufficiently about the chemical equilibrium processes which govern the composition of our films. As a consequence, it was not possible to obtain films with very high resistivities. Furthermore, it was not possible to obtain a good correlation between our electron microprobe composition analyses and the resistivities measured.

#### 2.5.2 Microwave Loss Measurements

The microwave loss factor  $\tan \delta$  was measured in selected samples for which dc resistivity measurements were also made. The results were compared with expected values due to conduction in the ferrite material. The ferrite films measured turned out to be extremely lossy and, although the loss factor decreased with increasing resistivity, it did so at a much smaller rate than expected due to electronic conduction (Figure 36).

Dielectric loss factors were measured at 9 GHz using the cavity perturbation technique. No applied magnetic field was used since the presence of a field away from ferromagnetic resonance did not alter the dielectric loss in the material. The rectangular waveguide cavity arrangement used is depicted schematically in Figure 34. Samples grown on alumina and glass substrates were measured; they were cut in 1-mm-wide strips for insertion into the cavity.

Figure 35 is an example of the raw data obtained for a sample film on alumina. The film is 2  $\mu\text{m}$  thick and has a resistivity  $\rho = 4000 \Omega\text{-cm}$ . Once the trace with the film was obtained, it was etched from the 1-mm-wide substrate, which was measured again in the cavity as the



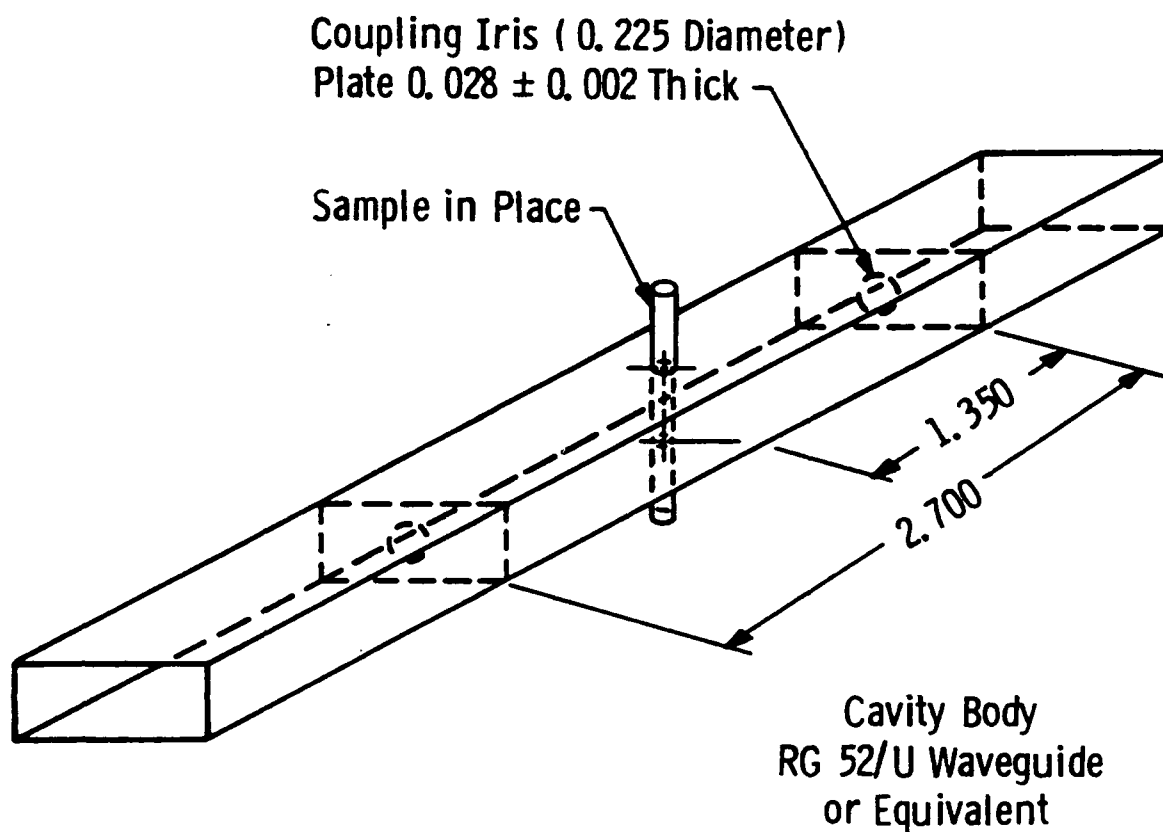


Figure 34. Schematic diagram of the experimental arrangement for dielectric loss measurements at 9.3 GHz. Measurements were made by comparing the film on its substrate with the substrate alone, after etching the film away.

Curve 758115-A

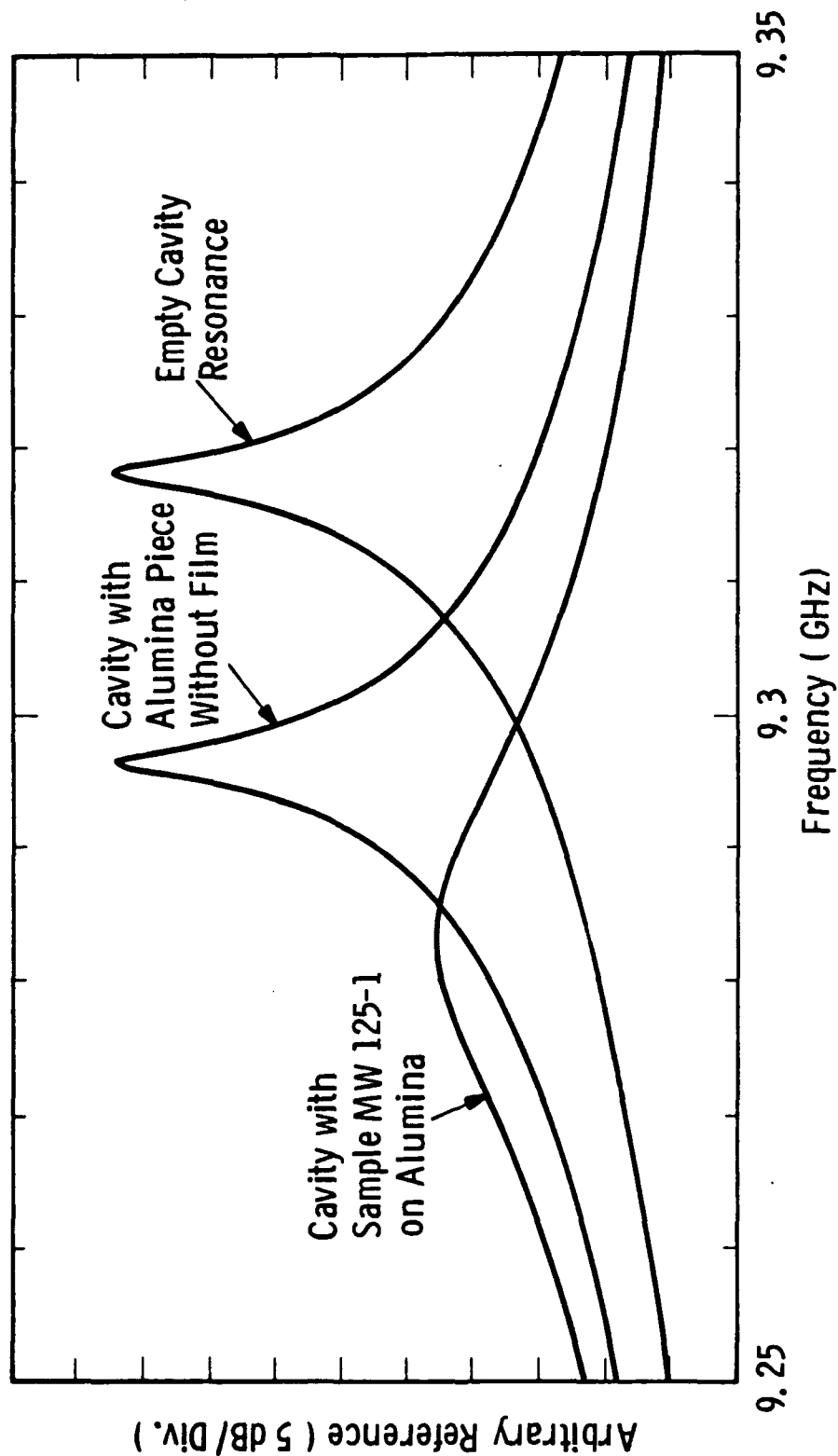


Figure 35. Example raw data from a  $\tan \delta$  measurement of a 2- $\mu\text{m}$ -thick ferrite film. The film has a dc resistivity of 4000  $\Omega\text{-cm}$ .

unperturbed reference. The real and imaginary parts of the dielectric constant can be extracted from the perturbed cavity data. They are proportional to the resonance frequency shift and the change in  $Q$ , respectively.<sup>8</sup> Because the films were so lossy and the cavity was so greatly perturbed, the resonance frequency was pulled away from the unperturbed reference farther than it would have been due to only the film (real) dielectric constant. The loss factor  $\tan \delta$  was therefore obtained approximately by assuming a real part of the dielectric constant of 12 (the literature value for Ni-Zn ferrite). The imaginary part was assumed to be equal to the value for lightly perturbed cavities, i.e., proportional to the change in  $Q$  of the cavity:

$$\epsilon'' = \frac{1}{4} \frac{v_c}{v_s} \delta \left( \frac{1}{Q} \right) \quad (4)$$

where  $v_c$  and  $v_s$  are the volumes of the cavity and the sample, respectively, and  $\delta(1/Q)$  is the difference in  $1/Q$  with and without the film, respectively. The loss tangent was then taken to be:

$$\tan \delta = \frac{\epsilon''}{\epsilon'} \quad (5)$$

with  $\epsilon' = 12$ .

With these assumptions, the plot of  $\tan \delta$  versus resistivity given in Figure 36 was generated from the samples measured. The dotted line is a calculation of  $\tan \delta$  versus resistivity for the case of microwave losses generated by conduction mechanisms alone. For comparison purposes only, Figure 37 is also included, the result of  $\tan \delta$  measurements on silicon material of different resistivities, performed on an unrelated program.<sup>9</sup> Notice that the loss factor is very close to the calculated value for relatively low resistivities. As the material becomes more insulating, the dominant loss mechanism is other than conduction.

Going back to Figure 36 then, it is quite clear that the dominant loss mechanism in our samples is much stronger than conduction, although, as seen from the plot,  $\tan \delta$  diminishes slowly with increasing resistivity. The first candidate cause for the observed high losses is

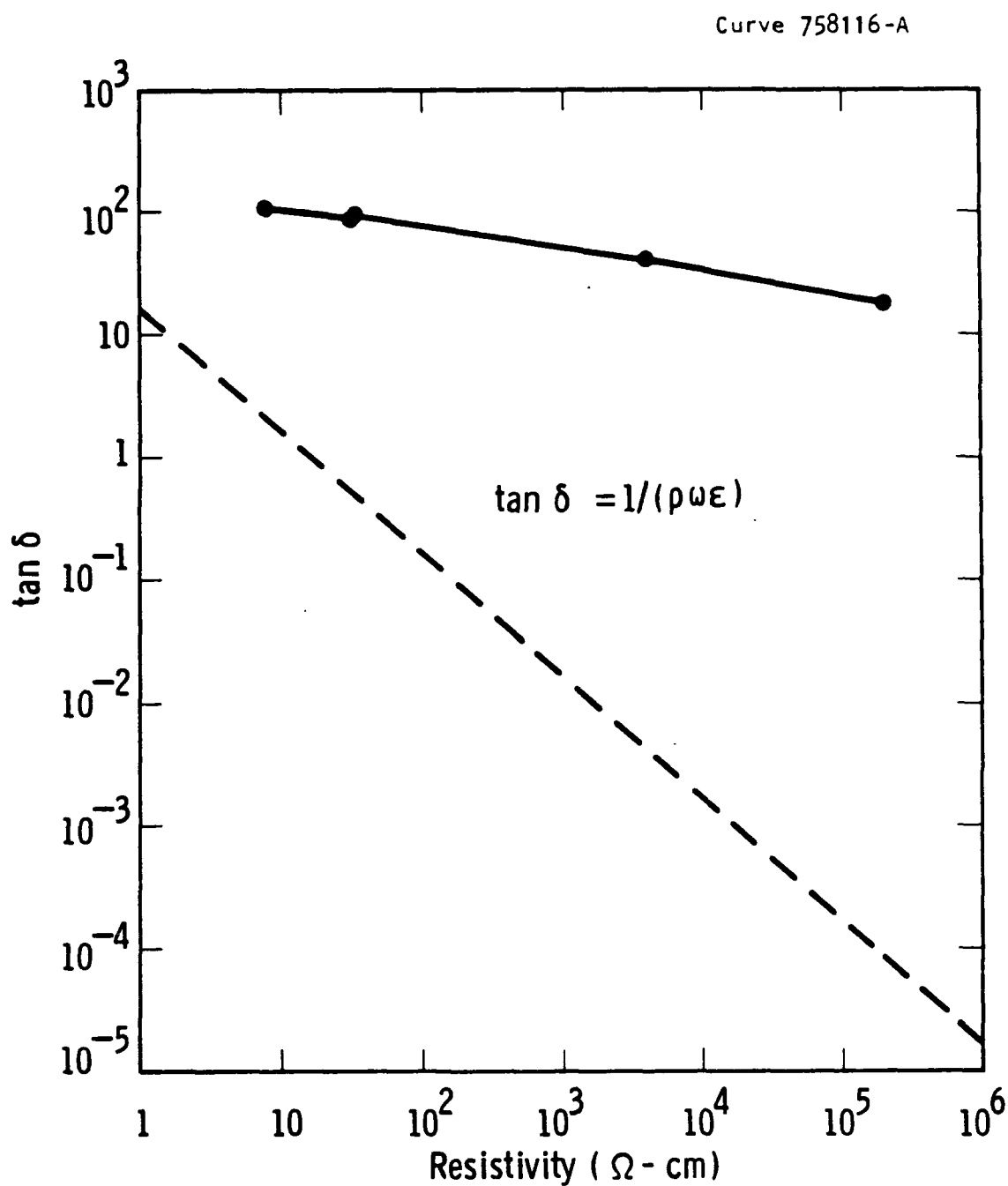


Figure 38. Dielectric loss tangent at 9.3 GHz as a function of dc resistivity for SSP Ni-Zn ferrite films.

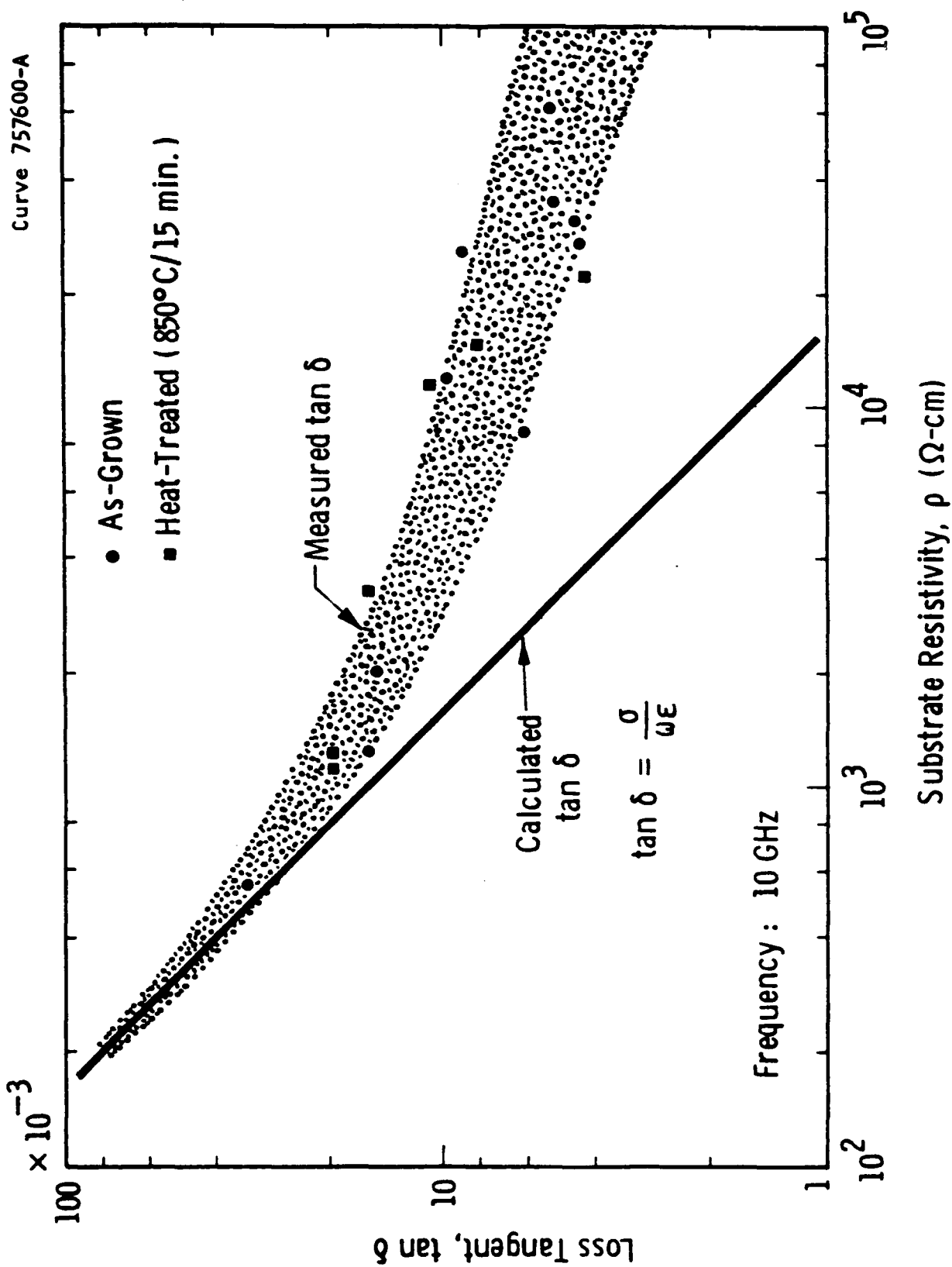


Figure 37. Loss tangent at 10 GHz versus dc resistivity for silicon material. Generated in an unrelated program,<sup>9</sup> this curve is included here for comparison with our results only.

water in our films, given the nature of the SSP deposition process. Preliminary work on drying our films, performed on internal funds immediately after the technical conclusion of this program, revealed that, indeed, there is an improvement in the loss tangent when the water content in the films is reduced. The drying process has not been optimized as yet; however, the indications so far are quite promising for films which at least will have no other loss but that caused predominantly by conduction due to incomplete substitution of Ni and Zn for divalent Fe.

## 2.6 CONCLUSION

The work on this part of the program has covered a very wide range of aspects related to the feasibility of using SSP ferrite films for monolithically integrated millimeter-wave electronic and magnetic devices. Most of the problems posed by this goal have been solved or have been demonstrated to be solvable with a limited amount of further work. That there are still problem areas that need attention does not detract from the merits of the spin-spray plating approach.

Two of these areas need immediate attention before a convincing device demonstration can be carried out. First and most urgently, the high microwave losses must be reduced to an acceptable level, and the apparent high water content in the films must be eliminated. The process developed for this purpose must be integrated with that for the growth of multilayer thick films. For example, growth of layers of optimized thickness should be alternated with suitable drying cycles to avoid trapping water with its associated losses.

Second, the chemical equilibrium conditions that control the composition of films must be understood and controlled. This difficulty is not as urgent as the one discussed above; a device demonstration could presumably be carried out before this problem is addressed. However, control of composition will be important once films with more reasonable microwave losses can be grown and device performance becomes the focus of attention.

Trapped water vapor may also cause problems when building up a very thick multilayer structure.

### 3. SPUTTERING OF BARIUM FERRITE THIN FILMS

#### 3.1 INTRODUCTION

The goal of this task was to produce oriented polycrystalline films of Ba-hexaferrite on GaAs wafers with c-axis texture perpendicular to the plane of the film. The sputtering technique offers the flexibility and capability of doing this, as demonstrated by Morisako et al. from Shinshu University in Japan.<sup>10</sup> The motivation for this task is that the high anisotropy fields of Ba-ferrite can be obtained with a sufficiently high degree of c-axis orientation without the need for epitaxial single-crystal film growth. High perpendicular anisotropy fields are required for device operation at millimeter wavelengths without having to apply impractically high bias magnetic fields.

At the beginning of this investigation, our approach was to reproduce the work of Professor Morisako,<sup>10</sup> who deposited c-axis oriented Ba-ferrite films onto substrates heated to 700°C, and improve upon same once accomplished. The improvements would be to allow deposition of films several microns in thickness on an encapsulated GaAs wafer coated with a layer of gold, which would serve as the ground plane for the magnetic device. More recently, work published by a group from Rockwell International<sup>11</sup> has pointed the way toward a desirable, parallel approach in which the sample is sputtered with the substrate heated at relatively low temperatures, followed by a post-deposition annealing to achieve c-axis orientation. The substrate deposition temperature was not well defined in the Rockwell paper, although they estimated it not to have exceeded 200°C. The annealing is done in oxygen at temperatures around 800°C. Of importance is the Rockwell group's report of very narrow ferromagnetic resonance (FMR) linewidths (<100 Oe) for their films at 60 GHz.

Both approaches require higher temperatures than GaAs devices can withstand; however, the effort was deemed worthwhile since deposition of the ferrite could be considered as a step prior to fabrication of the electronic devices.

### 3.2 FILM GROWTH

Figure 38 is a photograph of the RF sputtering equipment used in this work, a diode system arranged to sputter up. The system has an oil diffusion pump backed by a mechanical pump, is equipped with a liquid nitrogen trap, and is capable of producing a vacuum of  $10^{-6}$  Torr in the sputtering chamber. Additionally, the system is provided with a Meisner cooling coil that allows the chamber pressure to reach a value as low as  $10^{-7}$  Torr. This equipment was used mostly for direct deposition of c-axis Ba-ferrite films.

The second system used was a magnetron sputtering system arranged in a sputter-down configuration. It also has an oil diffusion pump backed by a mechanical pump and was used mostly for post-deposition annealed films. Both the RF-diode and the magnetron systems accept 75-mm diameter targets so they can be used interchangeably.

Targets with two different compositions were used in this work: a stoichiometric target of composition  $(\text{BaO})_6(\text{Fe}_2\text{O}_3)$  (i.e.,  $\text{BaFe}_{12}\text{O}_{19}$ , Ba-hexaferrite), and a Ba-rich target of nominal composition  $(\text{BaO})_{3.5}(\text{Fe}_2\text{O}_3)$ . Both were hot-pressed from powders. For films grown using diode sputtering, mostly the barium-rich target was used, whereas the stoichiometric target was used for magnetron sputtering.

Films were deposited by sputtering from the target in an argon and oxygen mixture. Their partial pressure, the total pressure, the substrate temperature, the substrate-to-target distance, and the RF power were all used as sputtering variables. Table 7 summarizes the range of these parameters. Post-deposition annealing of magnetron-sputtered films was carried out in oxygen ambient at 800-900°C. Quartz and silicon wafers (of several orientations) with a 2000 Å layer of thermal  $\text{SiO}_2$  on them were mainly used as substrates. Also used were platinum, in the diode-sputtering case, and sapphire, mainly for magnetron sputtering. Other substrates, such as a ZnO layer on  $\text{SiO}_2/\text{Si}$ , spinel, and  $\text{Ba}_3(\text{VO}_4)_{1.2}$ , have also been tried to a lesser extent in both sputtering experiments.

The films deposited were routinely characterized using X-ray techniques for orientation and composition. In addition, the composition of selected samples was analyzed by electron microprobe. Magnetic measurements using a vibrating sample magnetometer (VSM) and a torque





Figure 38. RF sputtering system used in this work.

Table 7  
RANGE OF DEPOSITION PARAMETERS

Parameter	Range
Total Pressure (mTorr)	6
Oxygen Partial Pressure	$1 \times 10^{-5}$ Torr - 1 mTorr
Power (Watts)	30 - 120
Substrate Temperature ( $^{\circ}\text{C}$ )	25 - 900

magnetometer (TM) were made on our best samples and on those sent to us by Professor Morisako from Japan. These measurements were made at Carnegie Mellon University by Professor J. O. Artman. Attempts to observe ferromagnetic resonance on any of the samples grown either here or in Japan failed, presumably because the resonance linewidths were broader than the upper limit of the (quite sensitive) equipment used.

### 3.3 RESULTS

Early in the program, communication was established with Professor Morisako, who sent us samples and, later, one of his targets. The substrate temperatures needed for deposition of oriented films were found to be around  $70^{\circ}\text{C}$  higher than those we used in the initial stages of this work. This was related to our slightly different way of monitoring the temperature. Also, it appeared that Morisako's target was of a higher quality than the one we used originally, which had been purchased from CERAC, Inc.

Figure 39(a) is an X-ray  $\theta/2\theta$  scan of a film deposited on quartz at a substrate temperature of  $630^{\circ}\text{C}$ , using our non-stoichiometric target. Interpretation of this pattern is at best ambiguous and only appears to indicate that the c-axis is laying on the plane of the film, instead of perpendicular to it. This result was typical of most depositions carried out using different conditions and substrates, but which had in common the lower-than-required substrate temperature and, perhaps, the lower quality of our target.

In sharp contrast to Figure 39(a) is Figure 39(b), which corresponds to a film highly oriented in the desired direction. This film was deposited on  $\text{SiO}_2/\text{Si}$  at  $705^\circ\text{C}$  using Morisako's target. We had previously obtained a similar epitaxial film on a platinum substrate which was directly heated by passing a current through it. X-ray oscillation photographs of this film and films grown on  $\text{SiO}_2/\text{Si}$  by Professor Morisako and us can be seen in Figure 40. This experiment was carried out to determine the range of substrate temperatures over which the oriented films can be obtained.

We concluded that both the better quality of the target and, above all, the higher substrate temperature accounted for the successful depositions onto  $\text{SiO}_2/\text{Si}$  substrates. Unfortunately, it was not possible to repeat the experiment beyond two runs; the substrate heater used was made from a flattened platinum wire which burned out after completion of the second run. Subsequent attempts at producing an adequate heater failed. It must be pointed out that growth of c-axis-oriented films seems to be extremely sensitive to contamination. When fabricating a heater it is important to achieve the high temperatures required without outgassing, which can prevent film growth with the desired orientation.

The best value for a half-width X-ray rocking curve for the RF-diode-sputtered films was  $2.3^\circ$ , which compares well with those obtained by Morisako.<sup>10</sup> The as-deposited films obtained by magnetron sputtering were amorphous and, on post-deposition annealing, became crystalline with the desired textured orientation. Figure 41 is the X-ray scan for our best film deposited using this approach. Films on  $\text{SiO}_2/\text{Si}$  were polycrystalline after annealing, whereas films on (0001) sapphire were epitaxial, as seen by the (000 $\ell$ ) peaks present in the X-ray scan (Figure 41). For substrate temperatures,  $T_s$ , less than  $200^\circ\text{C}$  and above  $500^\circ\text{C}$ , other orientations were observed. The half-width X-ray rocking curve for our best film, deposited at  $400^\circ\text{C}$ , was about  $0.68^\circ$  (insert, Figure 41), the smallest value reported so far in the literature. Figure 42 shows the variation of the rocking curve half-width as a function of  $T_s$ . This figure shows clearly that the optimum temperature is around  $400^\circ\text{C}$ , an observation that agrees well with that of Lacroix et al.,<sup>12</sup> who deposited oriented films on  $\text{SiO}_2/\text{Si}$  substrates at  $400^\circ\text{C}$  using RF targets-facing-type sputtering (TFTS). We could not, however, reproduce their result of obtaining oriented films on silicon

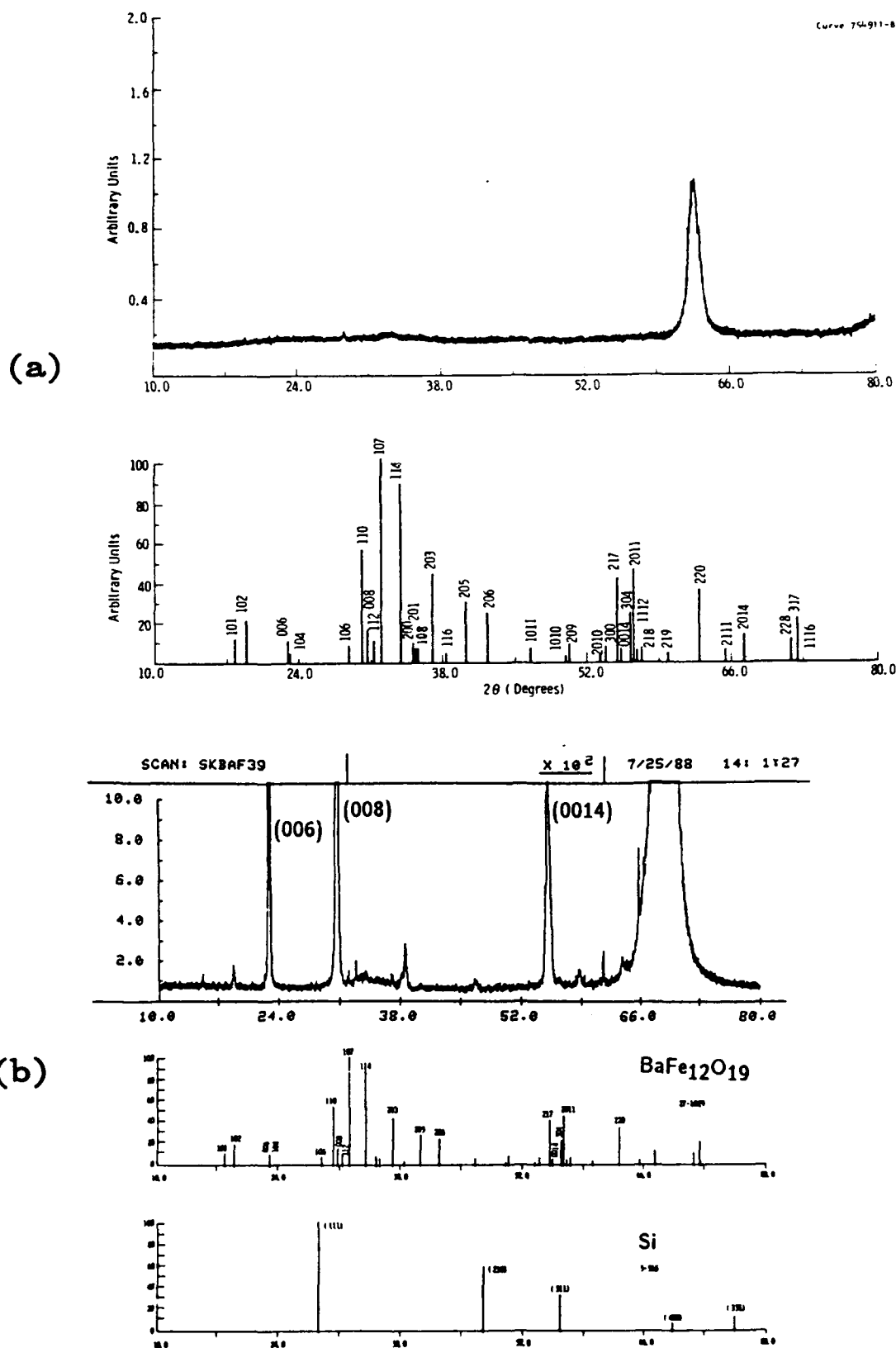


Figure 39. (a) Representative X-ray  $\theta/2\theta$  scan from sputtered sample BAF-7, and (b) X-ray  $\theta/2\theta$  scan of film BAF-39 showing c-axis texture. The large peak at  $69^\circ$  is due to silicon substrate.

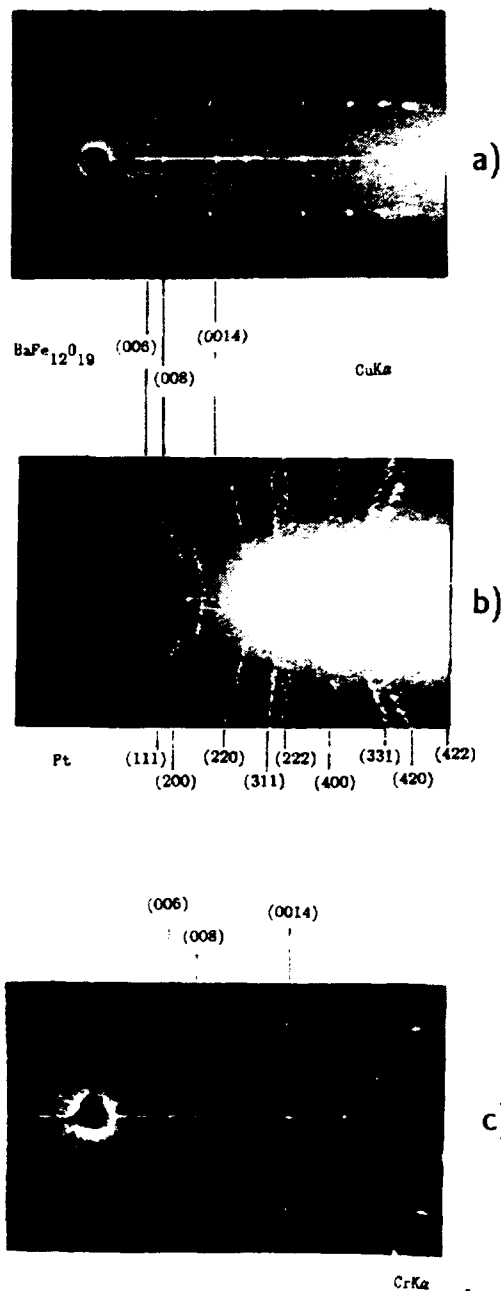


Figure 40. X-ray oscillation photographs of RF-diode-sputtered barium ferrite films taken with  $\text{CuK}\alpha$  radiation: (a) Film on  $\text{SiO}_2/\text{Si}$  grown by Prof. Morisako; sample BM-156. (b) Film on platinum grown at Westinghouse; sample BAF-35-2. (c) Film on  $\text{SiO}_2/\text{Si}$  grown at Westinghouse; sample BAF-39. It is clear from this photograph that using less-penetrating  $\text{CrK}\alpha$  radiation enhances the  $(00\ell)$  reflections.

Curve 758146-B

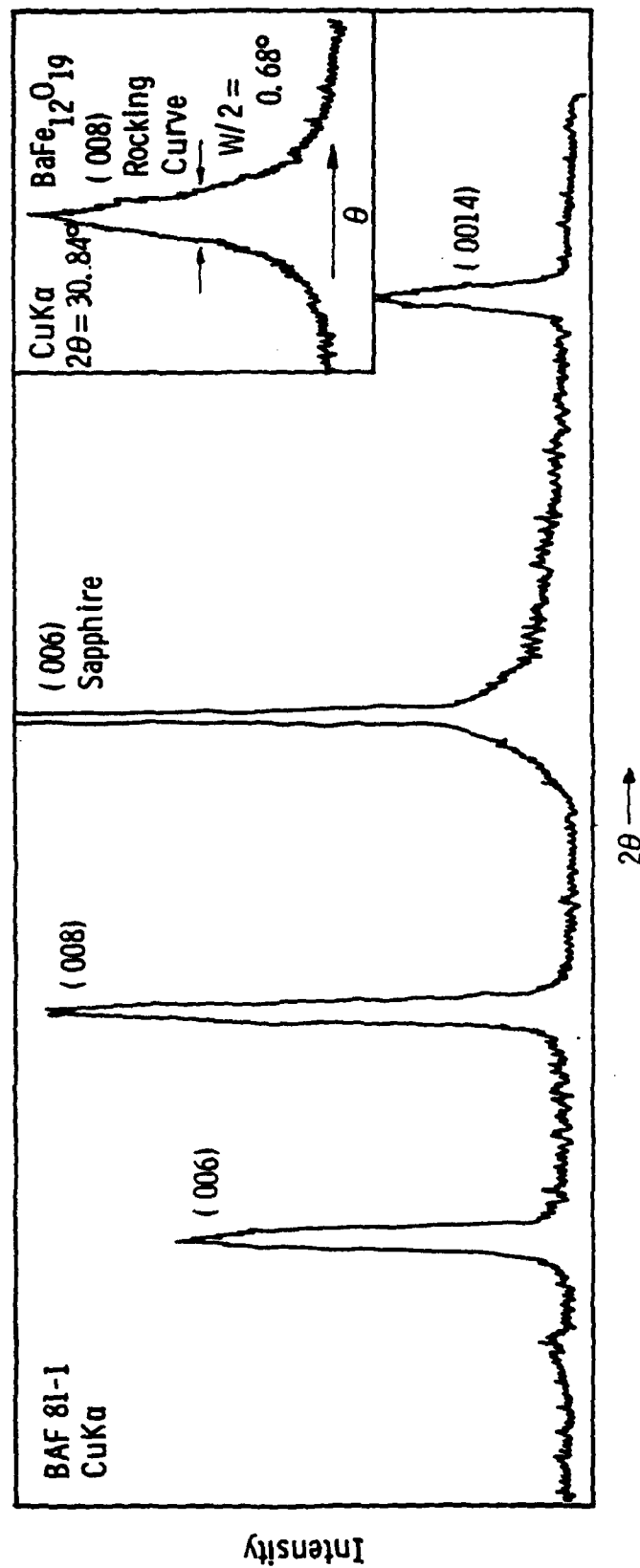


Figure 41. X-ray  $\theta/2\theta$  scan for magnetron-sputtered barium ferrite film on sapphire. Post-deposition annealing was carried out in oxygen at 800°C. Insert shows the rocking curve for this film.

Curve 758144-A

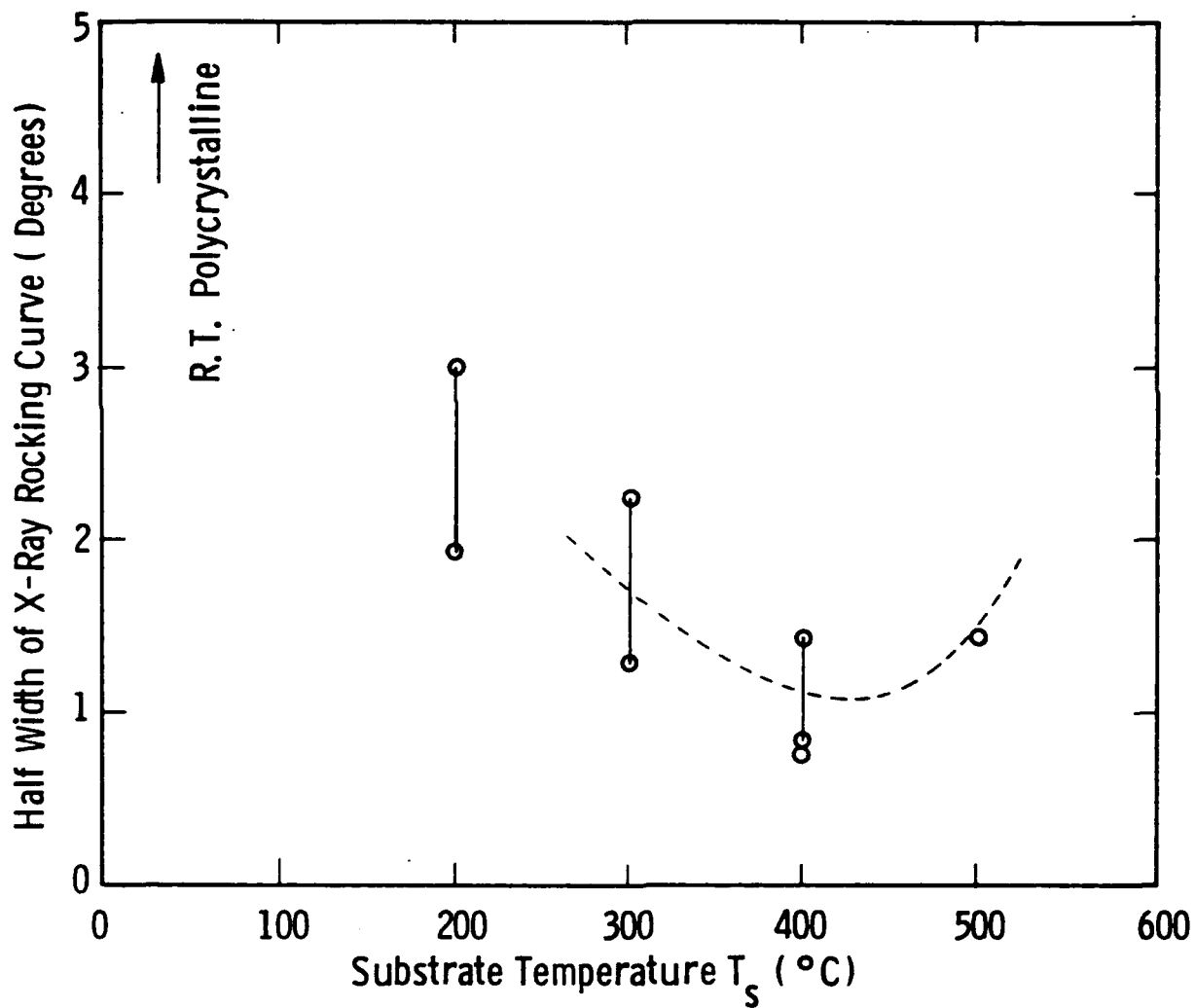


Figure 42. Variation of half-width X-ray rocking curve [(008) peak] for magnetron-sputtered films deposited at different substrate temperatures. CuK $\alpha$  radiation was used.

substrates even though we tried different orientations of silicon and different kinds (e.g., wet, dry, thermally grown, sputtered) of oxides. Increasing the post-deposition anneal time from 3 hours to over 16 hours did not improve the orientation for the films on sapphire and did not make the films on silicon substrates become oriented.

While a systematic study of the half-width spread with film thickness was not carried out in this work, preliminary indications are that thinner ( $<2000 \text{ \AA}$ ) films were very well oriented but, as the thickness increased, other orientations became significant.

Most of our film depositions in the magnetron system were carried out with an RF power of 30 watts. On the other hand, for most of the RF-diode depositions using the barium-rich target, the RF power was 120 watts. We also conducted room-temperature substrate deposition experiments in the RF-diode system, sputtering from the stoichiometric target at three different power levels: 30, 60, and 120 watts. The objective was to study the effect of RF power on film orientation. The films were deposited at room temperature onto sapphire substrates followed by a post-deposition anneal. While films deposited at 30 watts were polycrystalline with no preferred orientation, films deposited at 60 and 120 watts showed the c-axis in the plane of the substrate, seen by (110) and (220) peaks in the X-ray oscillation photographs taken.

### 3.3.1 Magnetic Measurements

Our best samples and those sent by Morisako were characterized magnetically by vibrating sample (VSM) and torque (TM) magnetometers. The results of this analysis, summarized in Table 8, yielded the saturation magnetization ( $4\pi M_s$ ) and the anisotropy field ( $H_k$ ). A relatively large margin of error exists in these measurements due to the difficulty in determining the effective area of the films on silicon substrates.

The sapphire pieces, on the other hand, were precisely cut to provide more accurate measurements for these samples. Moreover, a sapphire piece with no film was used to determine the background contribution from the substrate, and this was subtracted from the signal. Table 8 also lists the  $4\pi M_s$  and  $H_k$  values for bulk crystalline Ba-hexaferrite and shows that the  $4\pi M_s$  value for films on sapphire was better than that for films on  $\text{SiO}_2/\text{Si}$ . However, the anisotropy field was similar to that for films on other substrates and compares well with those reported by Morisako.<sup>18</sup>



Table 8

RESULTS OF ANALYSIS FROM VIBRATING SAMPLE AND  
TORQUE MAGNETOMETER MEASUREMENTS ON DIFFERENT  
SAMPLES OF SPUTTERED BA-FERRITE

Sample #	Substrate	RF Diode/ Magnetron	$4\pi M_s$ (KG)	$H_k$ (KOe)
BAF 39	SiO <sub>2</sub> /Si	Diode	1.52	10.00
BAF 40	SiO <sub>2</sub> /Si	Diode	1.60	9.20
BM 156*	SiO <sub>2</sub> /Si	Diode	1.725	-----
BM 144Nx	SiO <sub>2</sub> /Si	Diode	1.216	-----
BM 144Ax	SiO <sub>2</sub> /Si	Diode	2.886	-----
BAF 78	Sapphire	Magnetron	3.24	10.30
BAF 80	Sapphire	Magnetron	3.39	7.54
BAF 81	Sapphire	Magnetron	2.84	10.90
<hr/>				
BaFe <sub>12</sub> O <sub>19</sub> **			4.00	17.00

\* Samples with labels beginning with BM are from Prof. Morisako, Shinshu University, Japan.  $H_k$  was not measured in these samples.

\*\*von Aulock, Handbook of Microwave Ferrite Materials.

Figures 43 and 44 show examples of the raw data taken in these measurements, performed at Carnegie Mellon University by Professor J. O. Artman. They correspond to a film on sapphire grown at low temperature and annealed afterwards. Figures 43(a) and (b) are the perpendicular and parallel VSM traces. Of interest for microwave devices is the saturation magnetization that can be obtained more readily from the perpendicular trace. This value in Gauss is obtained by dividing the saturation in emu's from the trace by the volume of the sample in cm<sup>3</sup> (0.7 cm by 0.7 cm by 0.28 x 10<sup>-4</sup>) and multiplying the result by 4 $\pi$ . The parallel VSM trace is expected to be less square than the perpendicular one due to the anisotropy field perpendicular to the plane of the sample. The traces obtained by Morisako for his samples<sup>18</sup> are similar in shape, although in this case, ours had a higher  $4\pi M_s$ .

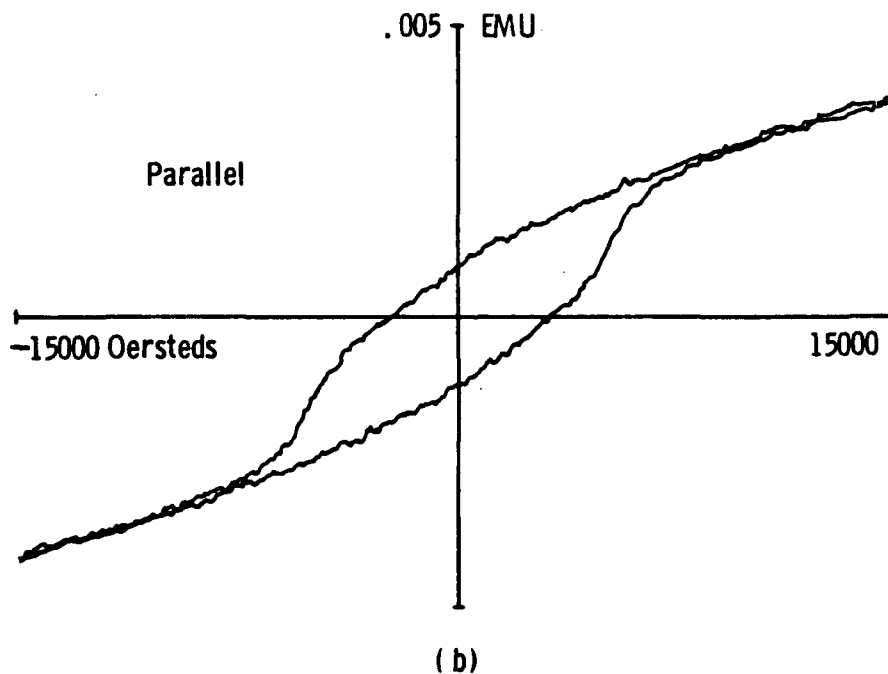
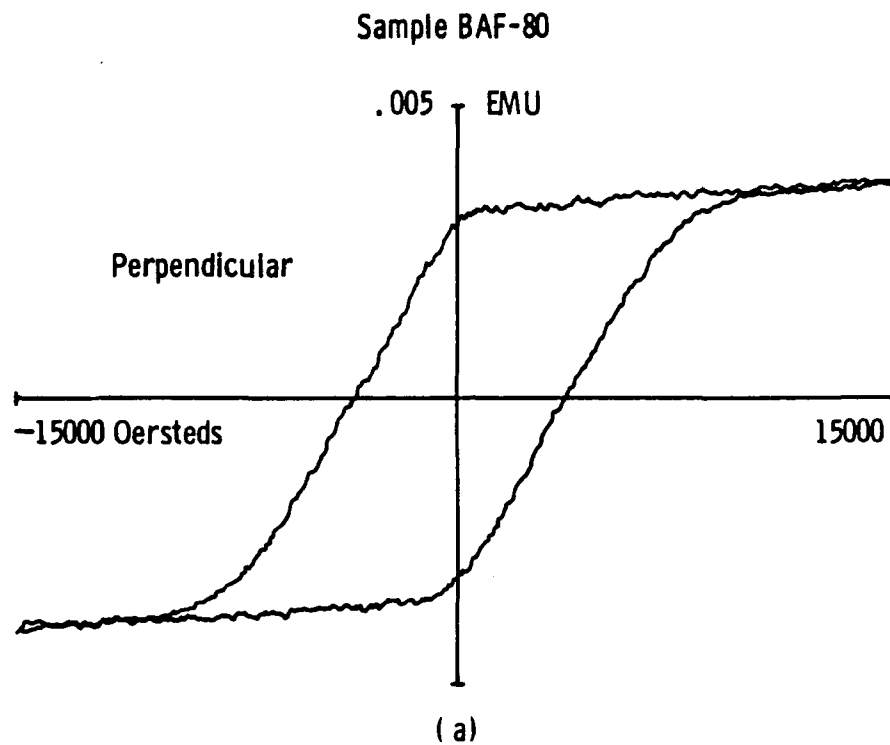


Figure 43. Vibrating sample magnetometer measurements: raw data for sample BAF-80 grown on sapphire by magnetron sputtering and post-deposition annealing. Film is 2,800 Å thick and sample measured was 7 mm by 7 mm. (a) Applied field perpendicular and (b) parallel to film plane.

Curve 758145-8

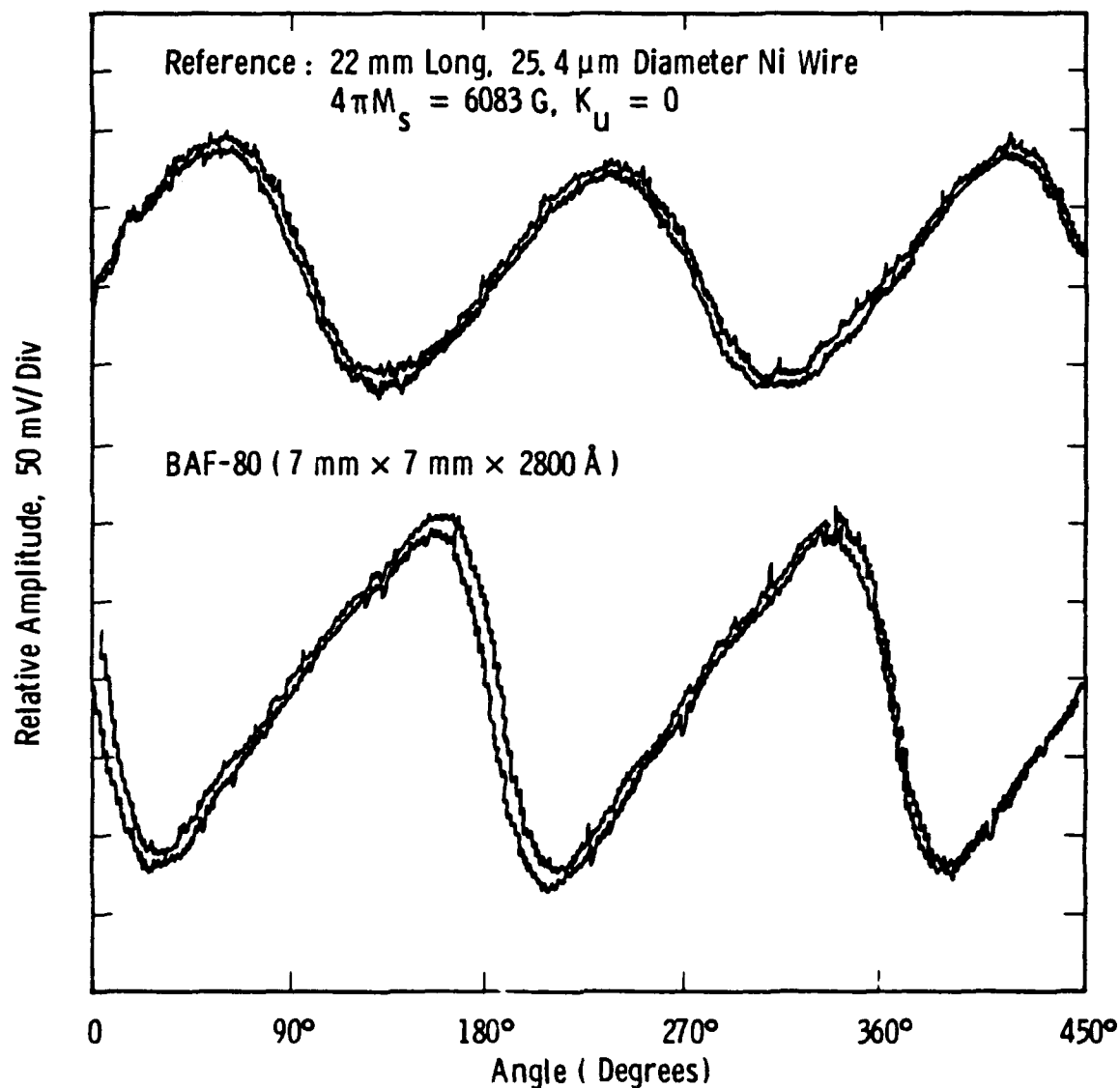


Figure 44. Torque magnetometer measurements: raw data for sample BAF-80 grown on sapphire by magnetron sputtering and post-deposition annealing. Film is 2,800  $\text{\AA}$  thick and sample measured was 7 mm by 7 mm. (a) Nickel wire reference and (b) BAF-80 sample.

Figures 44(a) and (b) are TM traces for (a) the reference, a nickel wire (0.005 cm in diameter by 2.2 cm in length;  $4\pi M_s = 6083$  G) magnetized perpendicular to its length, and (b) the same barium ferrite sample as for Figure 43. The measurement on the Ni wire gives a calibration for the amplitude of the trace, which is then compared to the amplitude obtained for the Ba-ferrite sample. This amplitude is a function of the perpendicular anisotropy field and the saturation magnetization. Thus, since the latter was obtained from the VSM measurement, the anisotropy field can be determined readily. Results for all the samples measured are summarized in Table 8.

It is very desirable to confirm these measurements with the FMR spectra, which also yields the resonance linewidth, of interest in microwave applications. It was not possible, however, to obtain FMR measurements on these films, probably due to very broad linewidths. Attempts were made both in-house at 50 GHz, and at Carnegie Mellon University at 33 GHz. The latter equipment is extremely sensitive, capable of measuring a ferromagnetic resonance linewidth 300 Oe wide in a 40-Å-thick oriented CoNiCr film on a glass substrate. In view of this, an attempt to improve the sensitivity of the FMR equipment available did not seem practical.

### 3.4 SUMMARY AND CONCLUSION

We have obtained highly oriented barium ferrite films on thermally oxidized silicon and sapphire substrates using RF-diode as well as magnetron sputtering techniques. Diode-sputtered films were deposited from a barium-rich target, and in-situ oriented films were obtained by holding the substrate at temperatures above 630°C. Magnetron deposition was carried out with substrates held at  $T_s < 400^\circ\text{C}$  and post-deposition annealing of the resulting films at 800 - 900 °C. A deposition temperature of 400°C appears optimum for growing structurally the best quality films. This is evidenced by the rocking curve half-width of 0.68°, the best value reported so far in the literature.

While in-situ oriented films on silicon substrates were obtained by RF-diode sputtering, we had to use Professor Morisako's target and even then the reproducibility was below our expectation. On the other hand, magnetron-sputtered films on sapphire were highly oriented and

obtained quite reproducibly. However, we could grow only randomly oriented polycrystalline films on silicon using this technique, even though others report growing oriented films on silicon by magnetron targets-facing-type sputtering. We believe both of these issues are related to the condition of our target. Indeed, our targets did not appear fully reacted, as seen from a small amount of  $\text{Fe}_2\text{O}_3$  found in some of our films as a second phase. While sapphire may be more forgiving and allow oriented growth to occur, such latitude may not be available during the nucleation stage for films on silicon substrates. We believe that future work should take this into account, and the target must be prepared from completely reacted material.

Although this work did not progress at the speed we had originally anticipated, the need for hexaferrite films compatible with desirable planar millimeter-wave magnetic device structures, not achieved as yet, promises gains commensurate with the risk and effort involved in producing these films. We have established the growth of highly oriented barium ferrite films and, having attained good reproducibility of film growth on sapphire, are confident it is possible to achieve characteristics suitable for millimeter-wave devices.

## 4. CONCLUSIONS

Two ferrite film deposition techniques were investigated in this program for possible use in the monolithic integration of GaAs electronic and magnetic millimeter-wave devices. Nickel-zinc ferrite films, grown by the spin-spray plating (SSP) technique, and barium hexaferrite films, deposited by sputtering, were considered as candidates for satisfying the goals of the program. The spin-spray plating was shown to be quite promising for this application, whereas sputtering of c-axis-oriented barium ferrite films fell somewhat short of our expectations. This is a difficult material to work with, and thin films for millimeter-wave work, epitaxial or even only with a texture orientation, are not yet widely available. Our results on Ba-ferrite films on sapphire substrates show that we have established a reproducible growth technique yielding a high degree of c-axis orientation in the direction perpendicular to the plane of the film. Further work is needed to produce thicker films which could be tested for their millimeter-wave properties. Films grown on this program had excellent structural properties, and vibrating-sample and torque magnetometer measurements gave acceptable saturation and anisotropy field parameters. However, it was not possible to observe ferromagnetic resonance in them, an important condition for millimeter-wave work.

SSP Ni-Zn ferrite films showed good structural and microwave magnetic characteristics. A broad range of aspects relating to their use for the goals of this program were investigated. Although all the problems were not solved, the technique's potential was clearly demonstrated. The most significant achievements and advantages of SSP are:

- The growth of Ni-Zn ferrite films was established. Film structural characteristics were studied, as well as their adhesion to various substrates and the conditions for growth of thick films.

- It was experimentally demonstrated that, since deposition of ferrite films takes place at 100°C, already fabricated GaAs devices would not be damaged.
- The SSP apparatus is very inexpensive and quite adaptable to production of a large number of wafers or deposition over large surfaces, planar or otherwise.
- The process for growing thick films suitable for practical devices and their feasibility was demonstrated.
- The magnetic characteristics of SSP Ni-Zn ferrite films are excellent for practical devices and quite comparable to published results on ceramic samples.
- A scheme for the monolithic integration of magnetic and GaAs electronic devices was put forth and its feasibility experimentally demonstrated.

The main problem areas encountered are the following:

- Ni-Zn ferrite films were found to have low resistivity and high dielectric loss at microwave frequencies owing apparently to high water content. A process to remove the water is under development with internal funding. Preliminary measurements on treated films show significant improvement in the microwave loss factor.
- Film composition cannot be controlled as readily as with ceramic samples due to chemical equilibrium conditions particular to the SSP process. These conditions are not completely understood as yet. The films grown in this program had only a partial substitution of Ni and Zn for divalent iron, which may result in unwanted residual microwave loss due to conduction.

Given the breadth of concerns inherent to establishing an ambitious new technology such as this, we believe the program was successful in demonstrating a new process for monolithic integration of magnetic and electronic devices. The original intention was that a junction circulator be demonstrated with this technology. This was not possible, however, due to the high loss in our films which, as explained, may be the result of high water content. Preliminary data show this to be a solvable problem.

As often occurs, we are limited by the laws of nature in our endeavor to make useful a certain physical system with desirable characteristics. Nevertheless, a potential solution was identified for almost all the problems encountered in this investigation.



## REFERENCES

1. M. Abe and Y. Tamaura, J. Appl. Phys. 55, 2614 (1984).
2. T. Takada and M. Kiyama, "FERRITES, Proc. of the Int. Conf.", p 69, July 1970.
3. W. H. von Aulock, Handbook of Microwave Ferrite Materials, Academic Press, 1965.
4. Trans-Tech, Inc. (Alpha Industries), Ferrite Type TT2-111:  $\gamma = 2.95$  GHz/KOe.
5. M. C. Driver, H. C. Nathanson, R. Freitag, G. W. Eldridge, R. C. Clarke and M. M. Sopira, "Wafer Scale Integration", IEEE Proc. Adv. Concepts in High Speed Semiconductor Devices and Circuits, Cornell U., Aug 1989.
6. J. Smit and H. P. J. Wijn, "Ferrites" John Wiley & Sons - Publishers (1959).
7. L. G. Van Uitert, J. Chem. Phys. 24, 306 (1956).
8. See for example, J. L. Altman, "Microwave Circuits", Van Nostrand, 1964.
9. Work performed at Westinghouse under U.S. Air Force contract no. F-19628-88-C-0114.
10. See for example, A. Morisako, M. Matsumoto and M. Naoe, Electronics and Communications in Japan, Part 2, 70, 55-65, 1987.
11. M. S. Yuan, H. L. Glass, and L. R. Adkins, Appl. Phys. Lett. 53, 340-341, 1988.
12. E. Lacroix, P. Gerard, D. Challeton, B. Rolland and B. Bechevet, J. de Physique, C8, 941-942, 1988.

## ACKNOWLEDGMENTS

The authors wish to acknowledge the technical contributions of S. J. Pieseski, D. W. Peters, P. E. Barbarich, and J. A. Kerestes.

**MISSION  
OF  
ROME LABORATORY**

Rome Laboratory plans and executes an interdisciplinary program in research, development, test, and technology transition in support of Air Force Command, Control, Communications and Intelligence (C<sup>3</sup>I) activities for all Air Force platforms. It also executes selected acquisition programs in several areas of expertise. Technical and engineering support within areas of competence is provided to ESD Program Offices (POs) and other ESD elements to perform effective acquisition of C<sup>3</sup>I systems. In addition, Rome Laboratory's technology supports other AFSC Product Divisions, the Air Force user community, and other DOD and non-DOD agencies. Rome Laboratory maintains technical competence and research programs in areas including, but not limited to, communications, command and control, battle management, intelligence information processing, computational sciences and software producibility, wide area surveillance/sensors, signal processing, solid state sciences, photonics, electromagnetic technology, superconductivity, and electronic reliability/maintainability and testability.